AGU PUBLICATIONS

JGR

Journal of Geophysical Research: Solid Earth

RESEARCH ARTICLE
10.1002/2013JB010716

Key Points:
- Large-volume plutonic rocks have lower magma fluxes than volcanic rocks
- Modeling indicates that zircon is unlikely to dissolve prior to supereruptions
- Zircon is a robust recorder of low fluxes in plutons and high fluxes in ignimbrites

Supporting Information:
- Readme
- Text S1
- Figure S1
- Figure S2

Correspondence to:
R. E. Frazer,
ryan.frazer@unc.edu

Citation:
Frazer, R. E., D. S. Coleman, and R. D. Mills (2014), Zircon U-Pb geochronology of the Mount Givens Granodiorite: Implications for the genesis of large volumes of eruptible magma, *J. Geophys. Res. Solid Earth*, *119*, 2907–2924, doi:10.1002/2013JB010716.

Received 24 SEP 2013
Accepted 26 MAR 2014
Accepted article online 29 MAR 2014
Published online 23 APR 2014

Zircon U-Pb geochronology of the Mount Givens Granodiorite: Implications for the genesis of large volumes of eruptible magma

Ryan E. Frazer[1], Drew S. Coleman[1], and Ryan D. Mills[2]

[1]Department of Geological Sciences, Mitchell Hall, University of North Carolina at Chapel Hill, Chapel Hill, North Carolina, USA, [2]Astromaterials Research and Exploration Science Directorate, NASA JSC, Houston, Texas, USA

Abstract The Mount Givens Granodiorite, a large pluton in the central Sierra Nevada batholith, California, is similar in area to zoned intrusive suites yet is comparatively chemically and texturally homogenous. New zircon U-Pb geochronology indicates that the pluton was constructed over at least 7 Ma from 97.92 ± 0.06 Ma to 90.87 ± 0.05 Ma. Combining the new geochronology with the exposed volume of the pluton yields an estimated magma flux of <0.001 km^3/a. The geochronologic data are at odds with the previously speculated links between plutons such as the Mount Givens Granodiorite and large-volume homogeneous ignimbrites (often termed monotonous intermediates). Existing data indicate that large plutons accumulate at rates of ≤ 0.001 km^3/a, 1–2 orders of magnitude less than fluxes calculated for dated monotonous intermediates. If monotonous intermediates are remobilized, erupted plutons accumulated at rates comparable to dated examples, they should preserve a record of zircon growth of up to 10 Ma. Alternatively, the long history of zircon growth recorded in plutons may be erased during the processes of reheating and remobilization that precede supervolcano eruption. However, zircon dissolution modeling, based on hypothetical temperature-time histories for preeruptive monotonous intermediates, indicates that rejuvenation events would not sufficiently dissolve zircon. We suggest that eruptions of monotonous intermediates occur during high magmatic flux events, leaving little behind in the intrusive rock record, whereas low fluxes favor pluton accumulation.

1. Introduction

Deciphering chemical, physical, and temporal relationships between intrusive and extrusive magmatic rocks is a fundamental issue in igneous petrology. Some large plutons and zoned intrusive suites are interpreted to either be unerupted crystal mushes or the crystalline residues left behind after large ignimbrite eruptions [*Hamilton and Myers*, 1967; *Hildreth*, 2004; *Bachmann et al.*, 2007a; *Lipman*, 2007]. In this hypothesis, both plutons and ignimbrites share the same histories as they are constructed incrementally as crystal-rich mushes over hundreds of thousands to millions of years. With no further inputs of magma, the mush may cool to form a granodiorite pluton. Alternatively, it is postulated that the mush may be rejuvenated by energy inputs, including underplating by basalts [e.g., *Mahood*, 1990]. This may cause remelting of crystals until the mush can convectively stir, leading to eruption as an unzoned, homogenous crystal-rich dacite, known as a monotonous intermediate [*Hildreth*, 1981].

In contrast, others suggest that voluminous intrusive rocks, such as those in large batholiths, do not share histories with comparable (volume and composition) ignimbrites. Plutons are hypothesized to accumulate mostly during low magma flux stages of long-lived volcanic centers. Ignimbrites are hypothesized to result from high magma input peaks that allow rapid production of voluminous melts, which are preferentially erupted and leave little behind in the plutonic record [*Glazner et al.*, 2004; *Tappa et al.*, 2011; *Zimmerer and McIntosh*, 2012a, 2012b; *Mills and Coleman*, 2013].

The composition, size, shape, and spacing of major intrusive suites led some workers to suggest a direct connection between these and large caldera-forming ignimbrites [*Lipman*, 2007; *Bachmann et al.*, 2007a; *de Silva and Gosnold*, 2007]. However, it is difficult to reconcile the genetic link between intrusive rocks and large ignimbrite eruptions because the existing data indicate different magma accumulation rates for the two. Emplacement rates for plutons and intrusive suites are in the range of 0.001–0.0001 km^3/a [*Crisp*, 1984]. In contrast, magma fluxes for large ignimbrites are typically at least an order of magnitude greater (greater than

0.01 km^3/a) [*Vazquez and Reid*, 2004; *Simon and Reid*, 2005; *Bachmann et al*., 2007b; *Wotzlaw et al*., 2013]. Numerical modeling of sill intrusion suggests that a magma flux greater than 0.005–0.01 km^3/a is required to create enough eruptible magma to feed supervolcano eruptions [*Annen*, 2009; *Gelman et al*., 2013; *Schöpa and Annen*, 2013].

One proposed solution to the magma flux dichotomy is the rejuvenation of high-crystallinity magmas that were accumulated slowly and stored in the upper crust. The most commonly invoked method of rejuvenation is an event during which mafic magmas underplate and "defrost" a silicic mush [*Mahood*, 1990]. As the mafic magmas crystallize, heat and volatiles may be released into the overlying mush. Various physical mechanisms that allow for heat transport, and thus rejuvenation, include convective self-mixing [*Couch et al*., 2001], gas sparging [*Bachmann and Bergantz*, 2003, 2006; *Huber et al*., 2010], and unzipping [*Burgisser and Bergantz*, 2011]. All of these mechanisms are hypothesized to result in resorption of crystals until they convect or stir [*Huber et al*., 2012], thus homogenizing the mush and allowing for eruption of a monotonous intermediate.

The Mount Givens Granodiorite (Figure 1) presents an opportunity to explore hypothesized relationships between plutonic and volcanic rocks. Though there are few volcanic rocks preserved in the Sierra Nevada batholith [*Bateman*, 1992] (for studies of direct comparisons see *Tappa et al*. [2011], *Mills and Coleman* [2013], *Rosera et al*. [2013], *Zimmerer and McIntosh* [2012a, 2012b], and *Zimmerer and McIntosh* [2013]), we examined the Mount Givens Granodiorite because this specific pluton is cited as an example of either the equivalent or residue of a magma body capable of generating a large-volume ignimbrite eruption. It has been compared to prominent calderas from which large ignimbrites erupted, such as the La Garita [*Bachmann et al*., 2007a], La Pacana [*de Silva and Gosnold*, 2007], and Toba [*Lipman*, 2007] calderas. The Mount Givens pluton is singled out because of its large volume (~4500 km^3) of texturally and compositionally homogenous granodiorite [*Bateman*, 1992] and because previous work on the pluton was undertaken with the notion that the magma was emplaced rapidly [e.g., *Bateman and Nokleberg*, 1978; *Tobisch et al*., 1993]. The longest estimates for its emplacement range from 10^3 to 10^6 annum [*McNulty et al*., 2000; *Petford et al*., 2000], suggesting fluxes on the order of 0.0045 to 4.5 km^3/a.

We use isotope dilution thermal ionization mass spectrometry (ID-TIMS) zircon U-Pb geochronology to evaluate magma emplacement rates in the Mount Givens Granodiorite and its possible link to caldera-forming eruptions. Furthermore, we use knowledge of the pluton's emplacement rate to evaluate models of crystal mush rejuvenation [e.g., *Bachmann and Bergantz*, 2003, 2006; *Burgisser and Bergantz*, 2011] and the effects rejuvenation may have on zircon dissolution. Geochronologic data are also useful in assessing the viability of existing hypotheses for the assembly of the Mount Givens pluton.

2. Geological Background

The Sierra Nevada batholith in California is a composite of mostly Cretaceous age granitoid plutons cropping out over approximately 35,000 km^2 (Figure 1) [*Bateman*, 1992]. Many of the plutons in the batholith are grouped into intrusive suites on the basis of their ages, spatial relations, compositions, and textures. Most intrusive suites in the Sierra Nevada batholith are characterized by having older, more mafic units at their margins and younger, more felsic units at their cores [*Bateman*, 1992]. Zircon U-Pb geochronology demonstrates that these suites were constructed incrementally over 7–16 Ma [*Coleman et al*., 2004; *Frazer et al*., 2009; *Davis*, 2010; *Memeti et al*., 2010; *Davis et al*., 2012; *Lackey et al*., 2012]. Individual mapped units within suites also show evidence for incremental growth over several Ma, including the Half Dome (at least 4 Ma, Tuolumne Intrusive Suite) [*Coleman et al*., 2004] and Lamarck Granodiorites (at least 3 Ma, John Muir Intrusive Suite) [*Davis et al*., 2012].

The Mount Givens Granodiorite is located in the central Sierra Nevada batholith, between the Shaver (106–98 Ma) [*Frazer et al*., 2009] and John Muir (96–84 Ma) [*Davis et al*., 2012] intrusive suites (Figure 1). Although originally included in the John Muir Intrusive Suite [*Bateman*, 1992], *Davis et al*. [2012] considered the Mount Givens pluton as distinct because it is separated from the rest of the suite by the Mount Goddard metamorphic pendant (Figure 1).

The Mount Givens pluton is one of the largest single intrusions mapped in the Sierra Nevada batholith [*Bateman*, 1992], extending approximately 80 km in its longest direction and between 15 and 30 km across (Figure 1). Whereas it is similar in area (1500 km^2) to the zoned Tuolumne and John Muir intrusive suites, published data indicate that compositional and textural variations in the pluton are not as significant as those

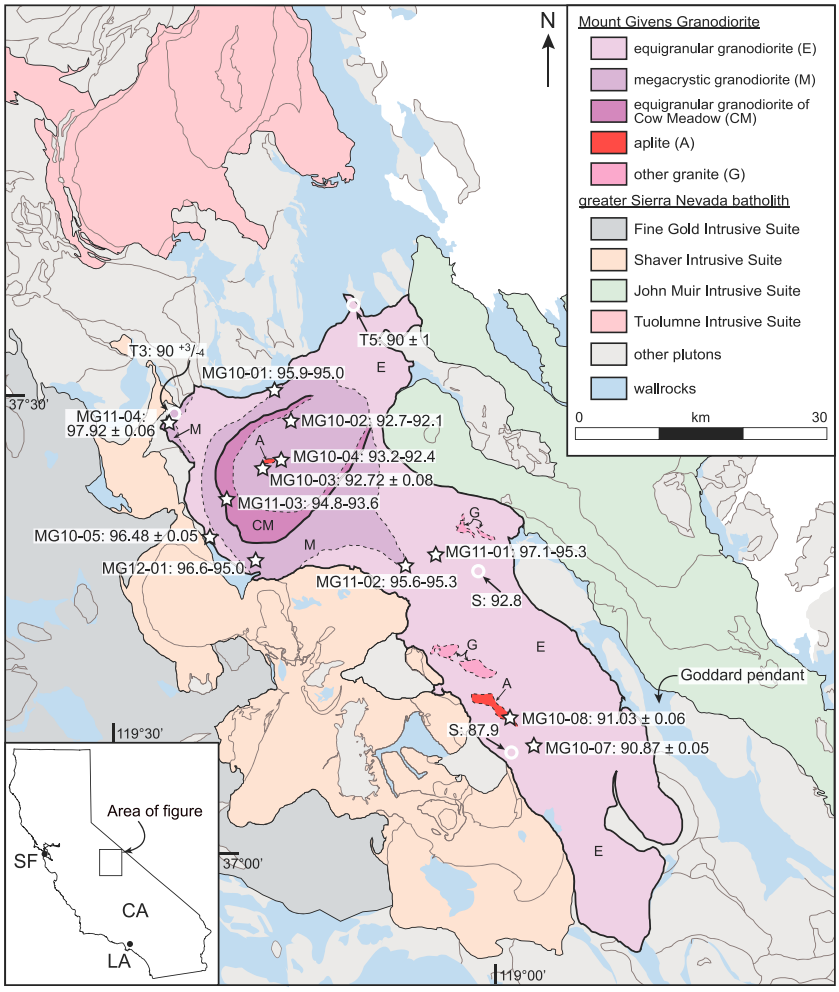

Figure 1. Simplified geologic map [after *Bateman*, 1992; *Lackey et al.*, 2008] of the central Sierra Nevada batholith showing approximate locations and ages (Ma) of samples dated in this study (stars) and in the literature (circles). Literature age prefixes: S, *Stern et al.* [1981]; T3, *Tobisch et al.* [1993]; and T5, *Tobisch et al.* [1995]. Thin dashed lines show gradational contacts; heavy black line on outer margin of the granodiorite of Cow Meadow indicates sharp intrusive contact [*Bateman et al.*, 1971; *Bateman*, 1992; *McNulty et al.*, 2000]. Plutons shown in light gray are not assigned to major intrusive suites. The John Muir Intrusive Suite of *Bateman* [1992] is modified after *Davis et al.* [2012]. CA, California; LA, Los Angeles; SF, San Francisco.

documented in the zoned suites [*Bateman and Nokleberg*, 1978; *Bateman and Chappell*, 1979; *Bateman*, 1992]. *Bateman and Nokleberg* [1978] examined the northern portion of the pluton and determined that most compositional variation occurs within 2 km of the margin. The composition of the pluton ranges from tonalite to granite, but granodiorite and granite dominate [*McNulty et al.*, 2000]. Small volumes of aplitic granite are exposed in the center of the exposed northern part of the pluton (granite of Jackass Rock) [*Bateman and Nokleberg*, 1978] and in the southern portion near Courtright Reservoir (Figure 1).

Whereas the southern two thirds of the pluton are dominated by equigranular granodiorite [*Bateman*, 1992], the bulbous northern end exposes both equigranular and megacrystic facies (Figure 1). The largest observed K-feldspar megacrysts are 3 cm long [*Bateman and Nokleberg*, 1978; *McNulty et al.*, 2000]. A horseshoe-shaped body of equigranular granodiorite (referred to herein as the granodiorite of Cow Meadow) [*Bateman et al.*, 1971] is found within the megacrystic facies and is mapped with a sharp outer contact and a gradational inner contact [*Bateman et al.*, 1971; *Bateman and Nokleberg*, 1978; *Bateman*, 1992; *McNulty et al.*, 2000]. All other contacts between textural and compositional phases are gradational [*Bateman and Nokleberg*, 1978].

Published zircon U-Pb ages for the Mount Givens Granodiorite range from 92.8 to 87.9 Ma [*Stern et al.*, 1981; *Tobisch et al.*, 1993, 1995]. However, these bulk zircon analyses are generally discordant and were not

Table 1. Zircon U-Pb Data for the Mount Givens Granodiorite[a]

Sample Fraction(n)	U (ppm)	Pb[b] (pg)	Th[c]/U	$^{206}Pb^{d}/^{204}Pb$	$^{206}Pb^{e}/^{238}U$	Error (2σ%)	$^{207}Pb^{e}/^{235}U$	Error (2σ%)	$^{207}Pb^{e}/^{206}Pb$	Error (2σ%)	Ages (Ma)[f] $^{206}Pb/^{238}U$	Ages (Ma)[f] $^{207}Pb/^{235}U$	Ages (Ma)[f] $^{207}Pb/^{206}Pb$	Correlation coefficient	Total[g] Common Pb (pg)
MG10-01 Equigranular Granodiorite, IGSN:P47000001[h] (*297825, 4153316*)[i]															
F-1(1)	925	131	0.40	2296	0.0149569	0.15	0.098870	0.30	0.047943	0.23	95.80	95.73	94.1	0.703	3.6
F-2(1)	942	65	0.38	1280	0.0148765	0.11	0.098447	0.36	0.047996	0.29	95.29	95.34	96.6	0.652	3.3
F-4(2)	798	120	0.42	6062	0.0149085	0.08	0.098773	0.20	0.048051	0.14	95.49	95.64	99.4	0.776	1.2
F-7(1)	1075	56	0.35	4490	0.0148374	0.09	0.098329	0.24	0.048064	0.20	95.04	95.23	100.0	0.578	0.8
F-8(1)	884	32	0.37	1613	0.0148271	0.12	0.098008	0.46	0.047941	0.39	94.98	94.94	93.9	0.628	1.3
F-11(1)	455	15	0.30	250	0.0144710	0.30	0.092861	4.89	0.046541	4.66	92.72	90.17	25.7	0.762	4.3
F-13(1)	381	32	0.39	721	0.0149323	0.12	0.100186	0.84	0.048661	0.78	95.64	96.95	129.1	0.531	2.8
F-14(1)	579	32	0.52	509	0.0149755	0.15	0.100116	2.18	0.048487	2.07	95.91	96.88	123.1	0.726	4.0
F-15(1)	243	23	0.57	285	0.0148902	0.23	0.099044	3.95	0.048242	3.77	95.37	95.89	111.2	0.780	5.1
F-17(1)	686	61	0.40	588	0.0149024	0.13	0.097693	1.92	0.047545	1.83	95.45	94.64	76.7	0.720	6.7
F-18(1)	663	23	0.43	399	0.0148576	0.19	0.099184	2.80	0.048416	2.66	95.17	96.02	119.7	0.739	3.8
MG10-02 Megacrystic Granodiorite, IGSN:P47000002 (*299119, 4150174*)															
F-1(1)	500	33	0.38	946	0.0144116	0.13	0.095834	0.75	0.048229	0.65	92.34	92.9	110.5	0.781	2.3
F-2(1)	144	13	0.58	261	0.0145260	0.17	0.097249	1.38	0.048555	1.28	93.06	94.2	126.4	0.612	3.2
F-3(1)	122	9	0.62	302	0.0142126	0.18	0.093262	1.38	0.047591	1.27	91.07	90.5	79.0	0.630	1.8
F-5(1)	552	42	0.39	915	0.0160376	0.21	0.107115	0.63	0.048441	0.56	102.66	103.3	120.8	0.477	3.0
F-6(1)	1137	79	0.45	3459	0.0143715	0.14	0.094943	0.31	0.047914	0.23	92.08	92.1	95.0	0.698	1.4
F-8(1)	801	43	0.53	281	0.0144038	0.12	0.095454	1.20	0.048064	1.16	92.28	92.6	102.4	0.421	9.9
F-9(1)	379	60	0.43	1532	0.0147726	0.13	0.098167	0.41	0.048196	0.34	94.63	95.1	108.9	0.657	2.5
F-10(1)	916	65	0.50	2077	0.0144685	0.09	0.095621	0.37	0.047932	0.32	92.69	92.7	95.9	0.685	1.9
F-11(1)	1219	115	0.40	4437	0.0144436	0.09	0.095453	0.28	0.047931	0.22	92.54	92.6	95.8	0.743	1.6
F-14(1)	353	50	0.48	2894	0.0150460	0.12	0.099761	0.30	0.048088	0.24	96.36	96.6	103.6	0.650	1.1
F-16(1)	194	13	0.48	112	0.0139247	0.34	0.092367	2.74	0.048109	2.67	89.24	89.7	104.6	0.275	8.7
F-19(1)	870	71	0.55	501	0.0146460	0.09	0.096941	0.54	0.048005	0.50	93.82	93.9	99.5	0.531	8.9
MG10-03 Aplitic Granite, IGSN:P47000003 (*295531, 4144923*)															
F-1(1)	1039	63	0.45	686	0.0144632	0.14	0.095646	1.64	0.047962	1.56	92.66	92.75	95.0	0.662	5.9
F-2(1)	1926	30	0.30	1302	0.0143436	0.12	0.094629	0.89	0.047848	0.83	91.91	91.81	89.2	0.540	1.5
F-3(1)	2470	74	0.49	3068	0.0144811	0.12	0.095723	0.45	0.047942	0.39	92.77	92.82	94.0	0.580	1.5
F-4(1)	801	34	0.48	2169	0.0144686	0.21	0.095590	0.83	0.047916	0.78	92.70	92.70	92.7	0.370	1.0
MG10-04 Megacrystic Granodiorite, IGSN:P47000004 (*296797, 4145483*)															
F-1(1)	759	152	0.50	6423	0.0145418	0.09	0.096238	0.30	0.047998	0.24	93.16	93.30	96.8	0.737	1.5
F-3(2)	1210	178	0.46	3985	0.0145225	0.09	0.095936	0.36	0.047912	0.31	93.04	93.02	92.5	0.593	2.8
F-4(2)	143	35	0.49	593	0.0141924	0.42	0.093821	1.95	0.047945	1.81	90.94	91.06	96.6	0.424	3.7
F-5(1)	79	33	0.46	2309	0.0144197	0.18	0.095656	0.63	0.048112	0.55	92.39	92.76	102.4	0.574	0.9
F-7(1)	735	230	0.44	4572	0.0144525	0.10	0.095354	0.31	0.047851	0.26	92.60	92.48	89.5	0.615	3.1
F-8(1)	244	16	0.44	1029	0.0139911	0.35	0.092420	1.62	0.047909	1.48	89.66	89.76	94.8	0.500	1.0
MG10-05 Equigranular Granodiorite, IGSN:P47000005 (*288528, 4136287*)															
F-1(1)	813	127	0.41	5359	0.0150762	0.10	0.099680	0.29	0.047953	0.23	96.56	96.48	94.6	0.654	1.5
F-2(1)	260	95	0.43	3913	0.0150419	0.12	0.099459	0.35	0.047956	0.29	96.34	96.28	94.7	0.583	1.5
F-4(1)	346	143	0.42	5401	0.0150703	0.10	0.099815	0.31	0.048037	0.26	96.52	96.61	98.7	0.601	1.7
F-5(1)	326	94	0.42	3896	0.0150850	0.11	0.100073	0.42	0.048114	0.38	96.61	96.84	102.5	0.508	1.5
F-6(1)	486	67	0.36	3461	0.0150641	0.21	0.099776	0.41	0.048038	0.32	96.48	96.57	98.7	0.638	1.2
F-8(1)	313	157	0.42	8078	0.0150334	0.12	0.099681	0.39	0.048090	0.29	96.29	96.48	101.3	0.872	1.2
MG10-07 Megacrystic Granodiorite, IGSN:P47000006 (*326375, 4110337*)															
F-1(1)	630	105	0.63	4132	0.0140661	0.11	0.092866	0.43	0.047883	0.37	90.13	90.17	91.1	0.629	1.5
F-2(1)	794	140	0.49	5744	0.0142037	0.11	0.093797	0.33	0.047895	0.26	91.01	91.03	91.6	0.662	1.5
F-3(2)	692	179	0.51	6079	0.0141690	0.10	0.093471	0.33	0.047845	0.30	90.79	90.73	89.2	0.360	1.8
F-4(2)	670	106	0.53	4422	0.0141938	0.14	0.093826	0.35	0.047943	0.29	90.95	91.06	94.0	0.617	1.5
F-7(1)	661	94	0.68	4624	0.0141691	0.11	0.093468	0.32	0.047843	0.27	90.79	90.73	89.2	0.615	1.2
F-8(1)	448	106	0.54	2761	0.0141963	0.32	0.093617	0.53	0.047827	0.39	90.96	90.87	88.3	0.676	2.3
MG10-08 Aplitic Granite, IGSN:P47000007 (*324733, 4113647*)															
F-1(1)	214	69	0.50	3171	0.0144541	0.11	0.095364	0.53	0.047851	0.47	92.60	92.49	89.5	0.646	1.3
F-2(1)	869	58	0.69	2441	0.0142028	0.12	0.093841	0.53	0.047920	0.48	91.00	91.08	93.0	0.511	1.4
F-4(2)	213	99	0.44	2952	0.0144315	0.10	0.094941	0.51	0.047714	0.46	92.46	92.10	82.6	0.596	2.1
F-5(1)	795	131	0.54	2364	0.0142060	0.11	0.093677	0.51	0.047825	0.46	91.03	90.92	88.2	0.516	3.4
F-6(1)	885	142	0.45	1087	0.0142266	0.15	0.093617	1.12	0.047725	1.04	91.16	90.87	83.2	0.590	8.3

Table 1. (continued)

Sample Fraction(n)	U (ppm)	Pb^b (pg)	Th^c / U	$^{206}Pb^d$ / ^{204}Pb	$^{206}Pb^e$ / ^{238}U	Error (2σ%)	$^{207}Pb^e$ / ^{235}U	Error (2σ%)	$^{207}Pb^e$ / ^{206}Pb	Error (2σ%)	Ages (Ma)[f] ^{206}Pb / ^{238}U	Ages (Ma)[f] ^{207}Pb / ^{235}U	Ages (Ma)[f] ^{207}Pb / ^{206}Pb	Correlation coefficient	Total[g] Common Pb (pg)
F-7(1)	230	39	0.82	280	0.0141723	0.27	0.093013	4.35	0.047599	4.17	90.80	90.31	79.4	0.685	8.4
MG11-01 Equigranular Granodiorite, IGSN:P47000008 (316480, 4132248)															
F-1(1)	442	107	0.38	3822	0.0151654	0.10	0.100390	0.38	0.048010	0.33	97.13	97.14	97.4	0.533	1.8
F-3(2)	1030	149	0.45	6859	0.0149696	0.10	0.099010	0.29	0.047970	0.23	95.88	95.86	95.4	0.655	1.4
F-4(2)	512	70	0.52	3327	0.0148840	0.17	0.098560	0.47	0.048026	0.40	95.33	95.45	98.3	0.579	1.3
F-9(1)	358	40	0.43	1069	0.0149655	0.11	0.099493	1.06	0.048217	1.01	95.85	96.31	109.9	0.549	2.4
F-10(1)	433	26	0.45	1503	0.0149555	0.11	0.099047	0.83	0.048033	0.76	95.79	95.90	100.9	0.666	1.1
MG11-02 Megacrystic Granodiorite, IGSN:P47000009 (312408, 4132076)															
F-1(1)	1288	140	0.25	1132	0.0158797	0.10	0.105097	0.97	0.048001	0.91	101.66	101.47	99.3	0.581	8.3
F-3(2)	898	121	0.45	6119	0.0149245	0.17	0.098938	0.36	0.048080	0.28	95.59	95.80	100.8	0.646	1.2
F-4(2)	431	84	0.44	3127	0.0149203	0.13	0.098721	0.44	0.047988	0.38	95.57	95.60	96.3	0.559	1.7
F-5(1)	459	190	0.30	7598	0.0148693	0.08	0.098008	0.22	0.047804	0.17	95.25	94.94	89.6	0.726	1.6
F-6(1)	407	36	0.42	1186	0.0149105	0.11	0.098744	0.97	0.048030	0.92	95.51	95.62	100.8	0.484	1.9
MG11-03 Equigranular Granodiorite, IGSN:P4700000A (290404, 4140734)															
F-4(1)	748	102	0.38	4655	0.0147711	0.09	0.097317	0.29	0.047783	0.24	94.62	94.30	86.1	0.639	1.4
F-5(1)	1483	114	0.34	788	0.0146037	0.13	0.096645	1.38	0.047997	1.31	93.56	93.68	96.6	0.572	9.5
F-6(1)	876	68	0.39	1579	0.0146228	0.20	0.096730	0.74	0.047976	0.67	93.68	93.75	95.6	0.469	2.8
F-10(1)	731	64	0.40	909	0.0147446	0.12	0.097589	1.23	0.048003	1.16	94.45	94.55	97.0	0.581	4.5
F-11(1)	768	127	0.39	883	0.0148002	0.10	0.097911	1.24	0.047981	1.17	94.81	94.85	95.9	0.662	9.2
MG11-04 Megacrystic Granodiorite, IGSN:P4700000B (283917, 4149984)															
F-1(1)	148	62	0.45	2107	0.0152836	0.10	0.101183	0.57	0.048015	0.52	97.87	97.87	97.7	0.520	1.8
F-2(1)	183	41	0.45	1906	0.0151892	0.15	0.101129	0.65	0.048288	0.59	97.27	97.82	111.1	0.494	1.4
F-3(1)	568	107	0.46	2657	0.0152857	0.18	0.101088	0.48	0.047964	0.41	97.89	97.78	95.2	0.537	2.5
F-4(1)	378	80	0.48	4339	0.0153928	0.09	0.101795	0.31	0.047963	0.26	98.57	98.43	95.2	0.636	1.1
F-7(1)	648	99	0.59	915	0.0152142	0.22	0.100699	1.27	0.048004	1.18	97.43	97.42	99.5	0.466	6.6
F-9(1)	480	38	0.47	1084	0.0152877	0.12	0.102085	1.02	0.048430	0.96	97.90	98.70	118.1	0.482	2.2
F-10(1)	276	61	0.58	2453	0.0152995	0.13	0.100639	0.59	0.047708	0.52	97.97	97.37	82.6	0.589	1.5
F-11(1)	140	23	0.42	739	0.0153064	0.15	0.101448	1.55	0.048070	1.48	98.02	98.11	100.4	0.532	2.0
F-12(1)	988	92	0.48	1370	0.0153625	0.14	0.101729	0.93	0.048027	0.86	98.37	98.37	98.3	0.595	4.2
MG12-01 Megacrystic Granodiorite, IGSN:P4700000C (294155, 4133495)															
F-5(1)	486	78	0.38	2381	0.0150753	0.11	0.099705	0.51	0.047968	0.46	96.55	96.50	95.3	0.510	2.1
F-6(1)	406	43	0.37	1285	0.0149142	0.10	0.098834	0.88	0.048063	0.82	95.53	95.70	99.9	0.550	2.1
F-7(1)	658	35	0.45	1469	0.0148360	0.11	0.098276	0.79	0.048043	0.74	95.03	95.18	99.0	0.535	1.5
F-9(1)	550	65	0.46	2038	0.0149060	0.10	0.098445	0.59	0.047900	0.56	95.48	95.34	94.3	0.386	2.0

[a] Pb blank ratios: $^{206}Pb/^{204}Pb = 18.687 \pm 0.25$; $^{207}Pb/^{204}Pb = 15.658 \pm 0.25$; and $^{208}Pb/^{204}Pb = 38.258 \pm 0.5$ (1σ abs.).
[b] Total mass of radiogenic Pb.
[c] Th contents calculated from radiogenic ^{208}Pb and the $^{207}Pb/^{206}Pb$ date of the sample, assuming concordance between U-Th and Pb systems.
[d] Measured ratio corrected for fractionation and spike contribution only.
[e] Measured ratios corrected for fractionation, tracer, and blank.
[f] Th-corrected isotopic dates calculated using the decay constants $\lambda_{238} = 1.55125E^{-10}$ and $\lambda_{235} = 9.8485E^{-10}$ [*Jaffey et al.*, 1971], assuming $Th/U_{magma} = 3.7$.
[g] Total mass of common Pb.
[h] IGSN = International Geo Sample Number. Access sample metadata, including collection and storage locations, at www.geosamples.org.
[i] Locations in NAD 83, UTM Zone 11.

determined using modern thermal annealing and chemical abrasion techniques [*Mundil et al.*, 2004; *Mattinson*, 2005]. Many workers consider the pluton to have intruded around 90 Ma [e.g., *Tobisch et al.*, 1993, 1995; *Renne et al.*, 1993; *Gilder and McNulty*, 1999; *McNulty et al.*, 2000]. All published models for the emplacement of the Mount Givens Granodiorite assume rapid (<1 Ma) intrusion of the entire body as either a single pulse [*Bateman and Nokleberg*, 1978; *Tobisch et al.*, 1993] or a series of dikes and sheets [*McNulty et al.*, 2000; *Petford et al.*, 2000].

3. Results

Analytical methods for zircon U-Pb dating (Text S1 in the supporting information) are given in the supporting information. Zircons from all samples contained few inclusions; the most common inclusions were apatite.

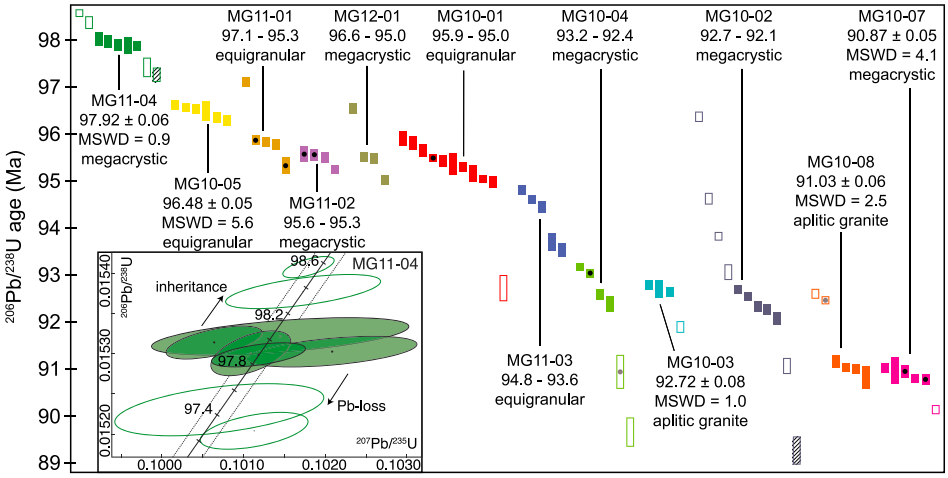

Figure 2. Compilation of new $^{206}Pb/^{238}U$ ages for zircon from the Mount Givens Granodiorite. All dates (in Ma) are concordant within analytical and decay constant uncertainties. All analyses presented are single zircons, except those indicated with a black circle, which include two zircons each. Ages given are our preferred interpretations for samples; see text for other interpretations. Analyses excluded from preferred interpretations are hollow. Weighted mean ages of samples MG10-07 and MG11-04 are used to determine preferred age range across pluton (~7 Ma). Hatched analyses (MG11-04 and MG10-02) indicate the age range when comparing only the youngest individual fractions between samples, assuming no Pb-loss (~8 Ma). For clarity, zircons F-5 (102.66 ± 0.22 Ma) from sample MG10-02 and F-1 (101.66 ± 0.22 Ma) from sample MG11-02 are not shown. Ages and 2σ analytical error calculated using the application U-Pb_Redux [*Bowring et al.*, 2011; *McLean et al.*, 2011]. All ages corrected for initial Th-disequilibrium assuming a magmatic Th/U ratio of 3.7. Inset shows an example of a concordia diagram for sample MG11-04, showing schematically how analyses affected by Pb-loss or inheritance are affected. Figure S2 contains concordia diagrams for other samples.

Cathodoluminescence images of representative grains from each sample (except MG10-03 and MG12-01, which were not imaged) indicate typical magmatic oscillatory zonation (Figure S1) [*Corfu et al.*, 2003]. Imaging also revealed the presence of possible inherited cores in some zircons; visual inspection suggests that MG10-01, MG10-02, MG10-04, MG11-01, and MG11-03 may have more frequent inherited cores than other samples. All data are concordant after correcting for initial Th/U disequilibrium (accounting for analytical and decay constant uncertainties; Table 1 and Figure 2). Many samples show scatter in individual zircon ages beyond analytical uncertainty.

3.1. Northern Part of the Mount Givens Granodiorite

Three of the four oldest samples were collected near the outer margins of the Mount Givens Granodiorite. The oldest sample, MG11-04, was collected near the northwest margin of the pluton in a small area mapped as megacrystic granodiorite, near the location of the 90 + 3/−4 Ma sample of *Tobisch et al.* [1993]. It has 2 cm K-feldspar megacrysts, the largest observed in any sample in this study. Five overlapping zircon ages yield a weighted mean age of 97.92 ± 0.06 Ma with a mean square weighted deviation (MSWD) of 0.9; the youngest zircon in that group has an age of 97.87 ± 0.10 Ma. Two zircons are about 500 ka older than the main grouping, and two zircons are about 500 ka younger.

Sample MG10-01 was collected from outcrop mapped as megacrystic facies at the northern margin, but the sample is equigranular. Ten individual fraction ages spread over 1 Ma of concordia, yielding a weighted mean of 95.37 ± 0.04 Ma with an MSWD of 25. One fraction is more than 2 Ma younger than the others. The youngest zircon in the large grouping has an age of 94.98 ± 0.12 Ma. Sample MG10-05 was collected at the western margin of the pluton. It is equigranular in texture, and six zircons yield a weighted mean age of 96.48 ± 0.05 Ma with an MSWD of 5.6; the youngest individual grain is 96.29 ± 0.11 Ma.

Samples MG10-02, MG10-03, MG10-04, MG11-03, and MG12-01 were collected inboard of the margins of the bulbous northern part of the pluton. The observed textures of all these samples matched the textures mapped for the sample locations by *Bateman* [1992] (Figure 1).

Sample MG11-03 was collected in the equigranular granodiorite of Cow Meadow near the mapped location of its intrusive contact with the megacrystic facies (Figure 1). However, the contact was not observed at the

sample locality. Five zircons range from 94.8 to 93.6 Ma, with one older cluster of three zircons (94.64 Ma ± 0.05 Ma; MSWD = 12) and one younger pair of zircons at about 93.6 Ma.

Samples MG10-03 and MG10-04 were collected approximately 1 km apart in the core of the northern part of the pluton. Sample MG10-03 was collected from the granite of Jackass Rock [*Bateman and Nokleberg*, 1978], a body of fine-grained aplitic granite. Three zircons overlap to give a weighted mean age of 92.72 ± 0.08 Ma with an MSWD of 1.0. Two zircons yield younger ages of 92.66 ± 0.13 Ma and 91.91 ± 0.11 Ma. Sample MG10-04, collected in the nearby megacrystic facies, has six fractions ranging from 93.2 to 89.7 Ma.

Sample MG10-02 is a megacrystic granodiorite. It yields a complicated age spectrum, with 12 concordant zircons ranging from 102.6 to 89.2 Ma. One cluster of five fractions yields a weighted mean age of 92.45 ± 0.05 Ma with an MSWD of 20; the youngest fraction in that cluster is 92.08 ± 0.13 Ma.

Sample MG12-01 is a megacrystic granodiorite collected adjacent to the spillway of the Mammoth Pool Reservoir in the area of the pluton's lowest exposed elevation. Four zircons yield an age spectrum from 96.6 to 95.0 Ma.

3.2. Central Part of the Mount Givens Granodiorite

Two samples, MG11-01 and MG11-02, were collected from the central part of the pluton. MG11-01 is an equigranular granodiorite; MG11-02 is megacrystic granodiorite. These two samples have ages that overlap with the marginal samples in the northern portion of the pluton. Sample MG11-01 yields five fractions ranging in age from 97.1 to 95.3 Ma; three overlapping fractions define a weighted mean age of 95.84 ± 0.06 Ma (MSWD = 0.8). Sample MG11-02 yields five fractions from 101.7 to 95.3 Ma; three overlapping fractions yield a weighted mean age of 95.54 ± 0.07 Ma (MSWD = 0.6). The youngest zircon fraction of that cluster is 95.51 ± 0.10 Ma.

3.3. Southern Part of the Mount Givens Granodiorite

Whereas the entire southern portion of the pluton was previously mapped as equigranular [*Bateman*, 1965, 1992], sample MG10-07 is megacrystic. Five fractions overlap for a weighted mean age of 90.87 ± 0.05 Ma and an MSWD of 4.1; the youngest zircon in that cluster is 90.79 ± 0.10 Ma. One fraction falls below the main grouping with an age of 90.13 ± 0.10 Ma.

Sample MG10-08 was collected from an area mapped as aplitic granite and is finer grained and more felsic than nearby granodiorites. It also contains 1 cm K-feldspar phenocrysts. Four zircons yield a weighted mean age of 91.03 ± 0.06 Ma (MSWD = 2.5), with a second group of two fractions near 92.5 Ma.

4. Discussion

4.1. Interpretation of Geochronologic Data

Improvements in analytical methods for ID-TIMS U-Pb zircon dating, including thermal annealing, chemical abrasion [*Mattinson*, 2005], and error treatment [*Schmitz and Schoene*, 2007; *McLean et al*., 2011], show that spread along concordia is a common occurrence in plutonic [e.g., *Coleman et al*., 2004; *Matzel et al*., 2006; *Tappa et al*., 2011; *Davis et al*., 2012; *Rioux et al*., 2012] and volcanic rocks [*Schoene et al*., 2010; *Meyers et al*., 2012]. The significance of analyses that are different from the main age group by several ka or more is unclear. Age dispersion can result from either (1) incomplete mitigation of Pb-loss, (2) diachronous zircon growth, (3) inheritance of xenocrystic or antecrystic zircon [*Miller et al*., 2007], or any combination of these three.

Despite the advancement of the chemical abrasion method [*Mundil et al*., 2004; *Mattinson*, 2005], high-precision U-Pb zircon studies continue to show cases of convincing Pb-loss (individual fractions far below main age groupings) [e.g., *Schoene et al*., 2010; *Meyers et al*., 2012]. For the zircon in this study, Pb-loss results in spread along concordia instead of apparently discordant ages as a consequence of the relatively young crystallization ages. Though we aggressively chemically abraded zircons in this study, there are several fractions far below the dominant age groupings or spreads in some samples (e.g., MG10-01, MG10-07) that we interpret to reflect Pb-loss, perhaps even Pb-loss that occurred during chemical abrasion in the laboratory.

Older ages within samples could be the result of prolonged (antecrystic) zircon growth in a crystal mush that was periodically rejuvenated by fresh magmas [*Miller et al*., 2007]. This scenario suggests a direct genetic link between older and younger zircons, which all grow at emplacement level. *Miller et al*. [2007] posited that

zircons might be recycled (and thus result in age spread in single samples) as high-crystallinity magmas mix with new inputs and zircons are redistributed throughout the crystal mush. Age overlap in the Mount Givens Granodiorite occurs between samples 1 km apart: sample MG10-03, an aplitic granite, is similar in age to sample MG10-04, a megacrystic granodiorite from which the aplite could have been derived. However, age spectra for samples from the margins (MG10-01, MG10-05, and MG11-04) and core of the pluton (MG10-03, MG10-04, and MG11-03) do not overlap. Consequently, the results suggest that if redistribution of antecrystic zircon occurred, it did not occur on the pluton scale and was likely limited to local mixing in younger samples.

Incorporation of zircons in ascending magmas prior to reaching emplacement level could also have contributed to the spread in zircon ages observed here [*Schaltegger et al*., 2009]. If magmas ascend rapidly [e.g., *Petford et al*., 2000] and cool quickly [*Davis et al*., 2012; *Rosera et al*., 2013], they may preserve inherited zircons incorporated during the ascent. Those zircons could be considered xenocrystic, since they could be foreign to the magma system that assembled the Mount Givens pluton. However, analyses contaminated by such inherited grains would not necessarily be discordant because much of the Sierra Nevada batholith is Cretaceous in age [*Bateman*, 1992], and therefore, inheritance moves analyses along concordia. Trace element analyses of zircons using the ID-TIMS-TEA method [*Schoene et al*., 2010] may be useful in helping determine the provenance of inherited zircons in future work.

There is an ongoing debate as to how complicated age spectra should be interpreted. Some workers choose to calculate weighted mean ages where possible, even if the MSWD values indicate geological scatter in ages outside of analytical uncertainty [*Coleman et al*., 2004; *Davis et al*., 2012; *Mills and Coleman*, 2013; *Rosera et al*., 2013]. In contrast, some workers choose to use the youngest interpreted closed-system zircon fraction to indicate the latest magmatic growth [e.g., *Schoene et al*., 2010; *Meyers et al*., 2012], though those particular studies were able to use stratigraphic order to judge the validity of that approach. We provide both weighted mean ages (including analytical uncertainty only) and youngest zircon ages for samples that contain populations of three or more overlapping analyses. However, we caution against the use of the youngest zircon in a grouping to indicate final crystallization here because we do not have stratigraphic or thermochronologic data to evaluate such an interpretation. In samples that do not have a distinct age group (e.g., MG10-04), we provide the full range of zircon ages that are clearly not a result of xenocrystic zircon or Pb-loss from oldest to youngest. Our preferred age interpretations are given in Figure 2. We note that 10 of the 79 analyses presented are two-zircon fractions (Table 1 and Figure 2), which can result in compression of age dispersion; however, these fractions represent a small portion of any individual sample and do not have a significant bearing on our age interpretations. For purposes of the discussion below, absolute age of the samples is less important than the range of ages recorded across the pluton. The range of our preferred ages is 97.92 ± 0.09 Ma to 90.87 ± 0.05 Ma (7 Ma). Using the youngest grains in each sample as indicative of emplacement age (assuming no analyses suffer from Pb-loss) yields a range from 97.27 ± 0.15 Ma to 89.24 ± 0.30 Ma (8 Ma), slightly younger but a slightly longer total range (Figure 2).

4.2. Assembly of the Mount Givens Granodiorite

Taken together, the zircon data for the Mount Givens Granodiorite require revision of models based on the assumption that it was assembled in less than 1 Ma [*Bateman and Nokleberg*, 1978; *Tobisch et al*., 1993; *McNulty et al*., 2000; *Petford et al*., 2000]. The data here are consistent with incremental assembly of the pluton over at least 7 Ma (approximately 98 to 91 Ma). There is little overlap between these new ages and previously published ages (92.8 to 87.9 Ma [*Stern et al*., 1981; *Tobisch et al*., 1993, 1995]). This may suggest an even longer period of assembly (~98–88 Ma) or may be the result of unresolved Pb-loss in the bulk zircon fraction analyses, which were completed before development of techniques to minimize this problem [*Mundil et al*., 2004; *Mattinson*, 2005].

Despite the significantly increased emplacement duration for the Mount Givens Granodiorite required by the data presented here, some aspects of existing emplacement models may be robust. For example, there is nothing in the data to contradict the suggestion of *McNulty et al*. [2000] that the pluton was assembled as a series of ascending dikes that spread laterally. In detail, however, their suggestion that different textural facies were intruded in discrete events is at odds with data demonstrating that assembly of the equigranular facies spanned at least 2 Ma and partially overlapped assembly of the megacrystic facies that spanned the entire 7 Ma range for the pluton. Also, the granodiorite of Cow Meadow is not the youngest part of the Mount Givens

pluton [*McNulty et al*., 2000]. Instead, the age range of its zircons falls between the ages at the margin and core of the pluton (Figure 2).

McNulty et al. [2000] found that magnetic foliations are subparallel to magmatic foliations observed in the field, which is a common observation [*King*, 1966; *Guillet et al*., 1983; *Cruden and Launeau*, 1994; *de Saint Blanquat and Tikoff*, 1997; *Cruden et al*., 1999; *Tikoff et al*., 2005]. They attributed magmatic and magnetic structures in the pluton to magma flow processes. However, the data presented here demand that the fabrics are diachronous and cannot reflect chamber-wide processes. Instead, recent work suggests such fabrics could be the result of crystallization in a thermal gradient [*Huang et al*., 2009; *Lundstrom*, 2009; *Lundstrom et al*., 2011] or realignment and recrystallization during thermal cycling [*Mills et al*., 2011].

4.3. Magma Fluxes in the Mount Givens Granodiorite

With the new geochronologic data for the Mount Givens Granodiorite, it is possible to estimate the flux of magma into the pluton's magma chamber. *Petford et al.'s* [2000] filling rate model for the Mount Givens pluton (0.032 km^3/a) was estimated without the benefit of multiple dated samples. Using the age range of the Mount Givens pluton established here (7 Ma), the area of the pluton (1500 km^2), and the exposed vertical relief as a proxy for thickness (3 km), we calculate an average magma flux for the Mount Givens Granodiorite of 0.0006 km^3/a. This estimate is similar to magma fluxes calculated for other plutons in the Sierra Nevada [*Coleman et al*., 2004; *Davis et al*., 2012; *Lackey et al*., 2012] and elsewhere [*Matzel et al*., 2006; *Tappa et al*., 2011; *Leuthold et al*., 2012; *Mills and Coleman*, 2013].

There is considerable uncertainty in calculating magmatic flux, but we consider our estimated average rate to be a maximum for the exposed portions of the Mount Givens Granodiorite for the following reasons: (1) the age range we use (98–91 Ma) is a minimum because it excludes zircons in several samples we interpret as affected by inheritance or Pb-loss; (2) unsampled rocks from other parts of the pluton could be older or younger than the range presented here, increasing the age range of the pluton and thus lowering the magmatic flux; and (3) the elevation variation of all samples in this study is ~1.8 km, whereas our magma flux is calculated using the total elevation variation in the pluton (3 km).

If the Mount Givens pluton's original volume were 33% greater due to a hypothetical 3:1 intrusive:extrusive ratio [*White et al*., 2006], its average flux would increase to only 0.0009 km^3/a. Using *McNulty et al.'s* [2000] thickness estimate of 5 km yields a flux of 0.001 km^3/a. However, we consider larger volume estimates for the purpose of magma flux calculations dubious because there is no a priori reason to assume that the crystallization ages of unexposed portions of the pluton will match those of the exposed portions. Neither the petrologic nor geochronologic relationships between unexposed/eroded rocks and the mapped pluton can be determined. Thus, the flux calculated is a maximum long-term average for the dated volume, unencumbered by estimates of the volume or age of unseen rocks.

Independent of the long-term average, the spatial distribution of the 12 samples dated here does not preclude the possibility that transient high flux events may be preserved in the Mount Givens Granodiorite. If high flux events occurred, those rocks are likely located in parts of the pluton where our sampling was less concentrated. The existing sampling and range of ages requires, however, that any high flux event be significantly less volumetric than the entire pluton. High-density sampling might reveal such an event; however, ID-TIMS dating is impractical for the number of samples required, and secondary ion techniques are too imprecise (±1–2% or 1–2 Ma at 100 Ma) to be of use.

4.4. Magma Fluxes in Plutons and Ignimbrites

The Mount Givens Granodiorite is cited as a possible intrusive analog to ignimbrites because it has similar composition, structure, and volume to large (>1000 km^3) homogenous crystal-rich dacites known as monotonous intermediates [*Bachmann et al*., 2007a; *de Silva and Gosnold*, 2007; *Lipman*, 2007; *Bachmann and Bergantz*, 2008]. On the basis of the similarity of their calculated intrusion rates for the Altiplano-Puna volcanic complex (0.012–0.06 km^3/a) to *Petford et al.'s* [2000] filling rate model for the Mount Givens pluton (0.032 km^3/a), *de Silva and Gosnold* [2007] suggested that pluton growth and large ignimbrite generation occur at the same rates and are thus directly linked. Although small-volume, high-flux episodes are permitted by the data presented here, the overall flux estimate challenges the link between processes responsible for

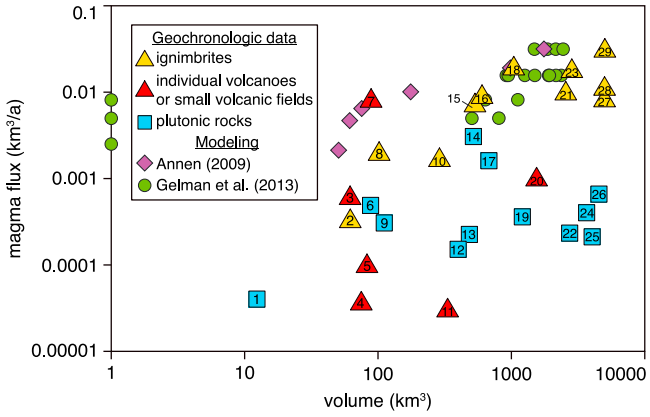

Figure 3. Compilation modified from *Mills and Coleman* [2013] of magma volume and flux estimates for intermediate and felsic plutons, individual volcanoes, ignimbrites, and modeling results. Modeling results from *Annen* [2009] and *Gelman et al.* [2013] are eruptible magma volumes. Data sources: 1, Lago della Vaca [*Schoene et al.*, 2012]; 2. Kos Tuff [*Bachmann et al.*, 2007c]; 3, Ceboruco [*Frey et al.*, 2004]; 4, Clear Lake [*Donnelly-Nolan et al.*, 1981]; 5, Ceboruco [*Frey et al.*, 2004]; 6, Torres del Paine [*Leuthold et al.*, 2012]; 7, Fuji [*Togashi et al.*, 1991]; 8, Rotoiti [*Charlier et al.*, 2003]; 9, Rio Hondo [*Tappa et al.*, 2011]; 10, Mesa Falls [*Bindeman et al.*, 2001; *Christiansen*, 2001; *Lanphere et al.*, 2002]; 11, Aucanquilcha [*Grunder et al.*, 2006]; 12, Tenpeak [*Matzel et al.*, 2006]; 13, Mount Stuart [*Matzel et al.*, 2006]; 14, Mount Stuart [*Matzel et al.*, 2006]; 15, Oruanui [*Wilson*, 2001; *Charlier et al.*, 2005]; 16, Bishop Tuff [*Hildreth*, 1979; *Simon and Reid*, 2005]; 17, Mount Princeton [*Mills and Coleman*, 2013]; 18, Lava Creek [*Bindeman et al.*, 2001; *Christiansen*, 2001; *Lanphere et al.*, 2002]; 19, Lamarck [*Davis et al.*, 2012]; 20, Davis Mountains [*Henry et al.*, 1994]; 21, Huckleberry Tuff [*Bindeman et al.*, 2001; *Christiansen*, 2001; *Lanphere et al.*, 2002]; 22, John Muir [*Davis et al.*, 2012]; 23, Toba [*Rose and Chesner*, 1987; *Vazquez and Reid*, 2004]; 24, Tuolumne [*Coleman and Glazner*, 1997; *Coleman* et al., 1997; *Bracciali et al.*, 2008; *Burgess and Miller*, 2008; *Memeti et al.*, 2010]; 25, Bass Lake [*Lackey et al.*, 2012]; 26, Mount Givens (this paper); 27, Fish Canyon [*Lipman*, 2000; *Bachmann et al.*, 2007b]; 28, Fish Canyon [*Lipman*, 2000; *Wotzlaw et al.*, 2013]; and 29, Fish Canyon [*Lipman*, 2000; *Schmitz and Bowring*, 2001].

assembling the Mount Givens Granodiorite and assembly of a shallow crustal proto-monotonous intermediate ignimbrite.

Numerical modeling by *Annen* [2009] indicates that constant magma fluxes greater than 0.01 km^3/a are necessary to develop magma chambers capable of supporting large (greater than 450 km^3) eruptions. In the case of variable magma fluxes through time, *Schöpa and Annen* [2013] found that a single, transient flux of greater than 0.05 km^3/a is required to generate more than 500 km^3 eruptible magma. Calculations by *Gelman et al.* [2013] refine previous models, taking into account varying thermal conductivity with temperature, suggesting that intrusion rates as low as 0.005 km^3/a may generate up to 500 km^3 of eruptible magma, though larger volumes require higher rates of input. These modeled magma fluxes are consistently higher than those calculated for intrusive rocks from geochronologic data. For example, even in the highly sampled Tuolumne Intrusive Suite (~30 ID-TIMS analyses across a similar volume and age range to the Mount Givens Granodiorite) [*Coleman and Glazner*, 1997; *Coleman et al.*, 2004; *Bracciali et al.*, 2008; *Burgess and Miller*, 2008; *Memeti et al.*, 2010], no sampled volumes within the suite meet the requirement of *Schöpa and Annen* [2013] that 500 km^3 be injected within 10 ka.

The suggested discrepancy between magma flux during pluton assembly and that required for the generation of large-volume ignimbrites is supported by existing geochronologic data (Figure 3). Whereas magma fluxes for intrusive and extrusive rocks are similar at small volumes, fluxes estimated for these rock types diverge at volumes greater than ~500 km^3. Plutonic rocks suggest assembly times of 10^6 to 10^7 annum for thousands of cubic kilometer of magma, whereas ignimbrites of comparable volume record zircon growth on the order of 10^5 annum. Likewise, thermal models show that large-volume plutonic rocks preserve average fluxes that are too low to generate supereruptions (Figure 3).

4.5. Zircon Dissolution During Mush Rejuvenation

The observation that phenocrysts in volcanic rocks often record heating events prior to eruption [e.g., *Bachmann and Dungan*, 2002; *Bachmann et al.*, 2002; *Wark et al.*, 2007; *Molloy et al.*, 2008; *Shane et al.*, 2008; *Bachmann*, 2010; *Wotzlaw et al.*, 2013] led to the hypothesis that monotonous intermediates and other large ignimbrite eruptions occur when long-lived, crystal-rich silicic mushes (50 + % crystals) are rejuvenated [e.g., *Mahood*, 1990; *Bachmann et al.*, 2002]. Though the proposed mechanisms by which the mushes may be revived differ [*Bachmann and Bergantz*, 2003, 2006; *Huber et al.*, 2009, 2010, 2012; *Burgisser and Bergantz*, 2011], the outcome—eruption—is the same. If heating events do not successfully rejuvenate a magma mush, then it may cool completely to form a granodiorite pluton [*Bachmann et al.*, 2007a].

Reconciling the connection between granodiorites and monotonous intermediates with the zircon geochronology of these rocks requires that zircons recording the multi-Ma history of growth of the mush be dissolved prior to eruption during the hypothesized thermal rejuvenation that initiates eruption [*Miller et al.*, 2007]. Thus, the long history of magma accumulation in the shallow crust is eradicated, and the short zircon growth history documented for ignimbrites reflects only the timescale of rejuvenation and eruption.

We test the hypothesis here using *Watson's* [1996, equation (17)] model for the instantaneous dissolution of a spherical zircon. We modeled the effects of heating events on zircons with initial radii from 10 to 150 μm, which are reasonable sizes for zircons in large ignimbrites [*Bindeman*, 2003]. Because the Mount Givens pluton is cited as a possible intrusive analog to the Fish Canyon Tuff [*Bachmann et al.*, 2007a; *Lipman*, 2007], parameters used were similar to those suggested for the Fish Canyon magma. Temperatures were increased from 715 to 760°C [*Bachmann and Dungan*, 2002] monotonically. Since proposed rejuvenation times range from less than a few centuries [*Burgisser and Bergantz*, 2011] to 200 ka [*Bachmann and Bergantz*, 2003; *Wotzlaw et al.*, 2013], we used the equation iteratively over timespans ranging from 1 ka to 200 ka. The dissolution equation is based upon peraluminous melts ($M \approx 1.3$, where $M \equiv (2\mathrm{Ca} + \mathrm{Na} + K)/(\mathrm{Si} \cdot \mathrm{Al})$), and although whole rock compositions of Fish Canyon Tuff have $M \approx 1.6$, interstitial glass inferred to represent liquid compositions has $M \approx 1.3$ [*Bachmann et al.*, 2002], making this equation appropriate.

In order to estimate the maximum dissolution possible, we began with the assumption of no dissolved Zr (0 ppm) in the melt initially, and any Zr derived from the dissolving zircons was immediately removed from the system (i.e., instantaneous infinite diffusion). Having initial Zr in the magma and/or increasing the Zr content of the magma in response to zircon dissolution in a limited reservoir would slow the dissolution process [*Watson*, 1996].

We tested our calculations against those in *Watson* [1996] and can replicate most of his results to within 2%. Over longer timespans, or *T-t* paths that reach much higher (up to 900°C) temperatures, we calculate shorter dissolution times than *Watson* [1996]. This is likely due to our use of *Watson's* [1996] simpler, iterative equation based on the "post-transient" phase of his moving boundary finite-difference solution. Thus, we take our results to be conservative minima for the amount of time necessary to dissolve zircons in these *T-t-X* conditions. Our (and *Watson's* [1996]) dissolution results are notably longer than similar published calculations by *Charlier et al.* [2005] and *Bryan et al.* [2008], even when differing temperatures and compositions are taken into account. However, the discrepancies can be explained by their use of a different magma viscosity model than *Watson* [1996] and a typographical error in their calculations for Zr diffusivity [B. Charlier and S. Bryan, personal communication].

Results suggest that it is possible to fully dissolve zircons with radii up to nearly 100 μm when variables are set to maximize zircon dissolution (Figure 4a). A heating event over 200 ka with no dissolved Zr present in the melt results in complete dissolution of the 10, 25, 50, and 75 μm radius model zircons. However, a zircon with an initial radius of 100 μm would survive the event with a final radius of 14 μm. Exposing zircons to the same temperature range using the shorter rejuvenation timespans (<1 ka) that were recently proposed [*Burgisser and Bergantz*, 2011] results in negligible dissolution (Table 2).

Predictably, the addition of Zr to the melt in this model results in less dissolution (Figure 4a and Table 2). With 60 ppm Zr held constant throughout the model (i.e., as the temperature increases, [Zr] is constant and the system becomes Zr undersaturated), the 75 μm radius zircon survives over 200 ka, whereas zircon of this size was dissolved in the Zr-free example. The addition of Zr also slows dissolution over shorter timescales; for example, the 10 μm radius zircon requires nearly twice as much time to fully dissolve when 60 ppm Zr is added. Similarly, using realistic (i.e., not infinite) melt reservoirs [*Watson*, 1996] would slow zircon dissolution.

If the rejuvenation event brings the temperature of the melt up to higher temperatures, more dissolution is possible. For example, if the temperature rises to 800°C (e.g., Lund Tuff) [*Maughan et al.*, 2002], larger zircons will dissolve over the longer time paths (Figure 4b). However, the increased temperature has little effect on zircons during the shorter rejuvenation events, and dissolution is further inhibited with the addition of Zr to the melt (Table 2).

Although previous work on the Fish Canyon Tuff suggests the system heated gradually to eruption temperature [*Bachmann et al.*, 2002; *Bachmann and Bergantz*, 2003], we briefly investigated the effects of incremental

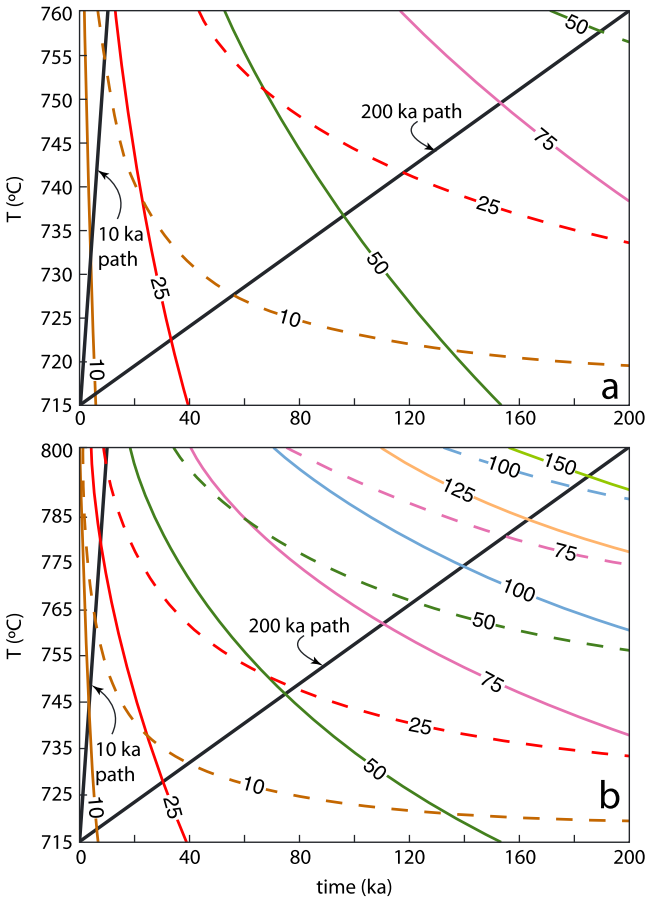

Figure 4. Temperature-time plots contoured for timing of dissolution of spherical model zircons (labeled with initial radii in μm) based on *Watson* [1996, equation (17)]. Contours indicate the *T* and *t* at which a zircon of a given radius fully dissolves assuming a linear *T*-*t* path beginning at the origin ($T = 715$°C; $t = 0$ ka). Solid colored contours show results determined with zero dissolved Zr in the model; dashed contour lines are for 60 ppm dissolved Zr held constant in the melt (see text). At any point below a given curve, that zircon survives without complete dissolution. Heavy black lines indicate a long heating path (200 ka) [*Bachmann and Bergantz*, 2003] and a short heating path (10 ka). Note that *Burgisser and Bergantz* [2011] suggest rejuvenation times <1 ka, which would not yield significant zircon dissolution. Any colored lines that intersect these paths indicate complete dissolution of model zircon. (a) Modeling based on the temperature range proposed for the Fish Canyon Tuff [*Bachmann and Dungan*, 2002]. Over the long heating path, zircons with radii <100 μm do not survive when no dissolved Zr is present, whereas 60 ppm Zr limits complete dissolution for zircons ≤50 μm. The 10 ka heating path only permits very small (<10 μm) zircons to fully dissolve. (b) Modeling with the upper temperature (800°C) based on maximum estimates for other monotonous intermediates [e.g., *Chesner*, 1998; *Lindsay et al.*, 2001; *Maughan et al.*, 2002]. Larger zircons dissolve than for the Fish Canyon Tuff, but short rejuvenation timescales will fully dissolve only the smallest (≤25 μm) zircons.

heating on zircon dissolution. Simulations where a high-frequency pattern of periodic heating and cooling is superimposed over a gradual trend from 715°C to 760°C or 800°C over 200 ka yield similar dissolution results to the monotonic heating models, regardless of [Zr] or initial radius. However, further study regarding the frequency and amplitude of temperature oscillations during rejuvenation events prior to ignimbrite eruption is necessary in order to better understand their effects on zircon behavior.

These calculations suggest that the effects rejuvenation events have on zircons may be limited, particularly because the parameters used in these models were chosen to maximize dissolution. For example, these models assume that the zircon is interacting with an infinite reservoir into which Zr may diffuse. However, in real systems the zircons likely interact with limited melt reservoirs (~1.5 mm radius), which would discourage dissolution [*Watson*, 1996]. Furthermore, the recent preferred timescales for rejuvenation of even the largest crystal-rich mushes such as the Fish Canyon Tuff are on the order of centuries to 10 ka [*Burgisser and Bergantz*, 2011; *Huber et al.*, 2012], which should preserve many of the initial zircons that would record mush growth (Figure 4 and Table 2).

These model results are supported by the presence of ancient xenocrystic zircon cores in monotonous intermediates [*Lanphere and Baadsgaard*, 2001; *Schmitt et al.*, 2002] and other large ignimbrites [*Zimmerer and McIntosh*, 2012a]. It is improbable that heating events preceding ignimbrite eruption would selectively dissolve zircons recording long-term (up to 10 Ma) growth of a "proto-ignimbrite" but would preserve much older zircons that were not derived from the active magmatic system. It is possible that ID-TIMS analyses on single zircons integrate subtle age variation from cores that represent early growth of zircon prior to reheating events. However, high spatial resolution ion microprobe studies mostly see variability of less than 0.4 Ma in zircon from ignimbrites [*Reid*, 2008], with rare exceptions [*Schmitt et al.*, 2002]. Furthermore, recent work on the Fish Canyon Tuff reveals synchronous U-Pb zircon

Table 2. Results of Spherical Zircon Dissolution Modeling[a]

r_o (μm)	1 ka	50 ka	100 ka	150 ka	200 ka
		715–760°C, 0 ppm Zr in Melt			
10	7.3	—	—	—	—
25	24.0	—	—	—	—
50	49.5	11	—	—	—
75	74.7	56	29	—	—
100	99.8	87	71	51	14
125	124.8	114	103	91	74
150	149.8	141	132	121	110
Max[b]	6.8	49	69	85	99
		715–760°C, 60 ppm Zr in Melt			
10	9.3	—	—	—	—
25	24.7	—	—	—	—
50	49.9	42	32	17	—
75	74.9	70	64	58	51
100	99.9	96	92	88	83
125	124.9	122	119	115	112
150	150.0	147	145	142	139
Max[b]	3.8	27	38	47	54
		715–800°C, 0 ppm Zr in Melt			
10	—	—	—	—	—
25	22.1	—	—	—	—
50	48.6	—	—	—	—
75	74.0	—	—	—	—
100	99.3	53	—	—	—
125	124.4	91	35	—	—
150	149.5	123	88	26	—
Max[b]	11.6	84	119	147	171
		715–800°C, 60 ppm Zr in Melt			
10	5.2	—	—	—	—
25	23.5	—	—	—	—
50	49.3	—	—	—	—
75	74.5	43	—	—	—
100	99.6	78	49	—	—
125	124.7	108	89	63	18
150	149.7	136	121	103	83
Max[b]	8.5	61	87	106	123

[a]Final radii (μm) of zircons calculated with the given parameters (r_o, temperature range, [Zr], and time period) using *Watson* [1996, equation (17)]. Dash denotes complete dissolution.
[b]Radius (μm) of the largest zircon that will completely dissolve using given parameters.

and $^{40}Ar/^{39}Ar$ sanidine ages, as well as pristine, unresorbed crystal faces on zircon, suggesting that zircon was crystallizing up until the time of eruption [*Wotzlaw et al.*, 2013]. In order for rejuvenation events in felsic and intermediate systems to successfully eradicate the zircon population, the events must be hot, long-lived, and very Zr-poor.

4.6. Estimating Volcanic Output Related to Emplacement of Large Plutons

The data presented here indicate that the difference in age spans between monotonous intermediates and plutons is related to different magma accumulation rates for the two; zircon is unlikely to be resorbed during the rejuvenation events suggested for monotonous intermediates. Thus, we suggest that the age range recorded by zircon in monotonous intermediates is indicative of high flux events that favor magma evacuation in large eruptions. These eruptions may leave little behind in the plutonic record, as evidenced by the lack of large volumes of cogenetic intrusive rocks with the tight age spans similar to those observed in ignimbrites [*Tappa et al.*, 2011; *Mills and Coleman*, 2013]. Conversely, the lower fluxes calculated for plutons are a reflection of the incremental emplacement of magmas that are preferentially stored in the crust, because they tend to cool rapidly after emplacement [*Annen*, 2009; *Davis et al.*, 2012; *Rosera et al.*, 2013; *Schöpa and Annen*, 2013]. Thus, whereas the composition and volume of the Mount Givens Granodiorite are

similar to those observed in large ignimbrites such as the Fish Canyon Tuff [*Bachmann et al.*, 2007; *Lipman et al.*, 2007], the rocks preserved apparently did not accumulate rapidly enough to generate a supereruption.

Recently, *Wotzlaw et al.* [2013] suggested that the Fish Canyon magma might have been up to 80% crystallized prior to rejuvenation, implying a connection between compositionally equivalent monotonous intermediates and granodiorite plutons. However, if the Fish Canyon magma successfully solidified after just ~220 ka of growth [*Wotzlaw et al.*, 2013], the resulting pluton would have accumulated at an average rate of 0.023 km^3/a, more than an order of magnitude faster than plutons of similar volume (Figure 3). This suggests that ignimbrite magma chambers preferentially erupt most of their content, perhaps due to temperature cycling with a shorter period and higher amplitude than plutonic units of similar size and composition.

It is possible that ephemeral high flux events may have occurred in or near parts of the growing pluton [*Schöpa and Annen*, 2013], perhaps even leading to the eruption of a large ignimbrite. However, if such an event (or events) occurred, it either resulted in near-complete evacuation of the magma, leaving little behind in the plutonic record, or is unsampled in existing detailed geochronology of plutonic rocks [*Coleman et al.*, 2004; *Matzel et al.*, 2006; *Davis*, 2010; *Memeti et al.*, 2010; *Davis et al.*, 2012; *Mills and Coleman*, 2013]. Thus, the chemical and volumetric similarities between plutons and ignimbrites do not necessitate a genetic relationship between the two; plutons need not be either unerupted ignimbrites or residues complementary to ignimbrites. Likewise, ignimbrites may not leave behind voluminous amounts of unerupted material as plutons. For example, the only exposed intrusive rocks in the Mount Aetna caldera coeval with the Badger Creek Tuff in Colorado are small-volume tuff dikes and ring dikes; larger-volume plutonic rocks bracket the tuff in age [*Mills and Coleman*, 2013; *Coleman et al.*, 2013]. Consequently, studies that use the ignimbrite record as a proxy for unexposed batholiths [*Bachmann et al.*, 2007a; *de Silva and Gosnold*, 2007; *Lipman*, 2007] should be viewed with caution; plutons may accumulate beneath regions of ignimbrite activity [*Zimmerer and McIntosh*, 2013], but they do not necessarily reflect the accumulation and/or eruptive processes of those events.

We suggest that potential magma output coming directly from the Mount Givens system could have resulted in arc stratovolcano activity. There are many similarities between pluton assembly rates and small-volume arc volcanic fluxes (Figure 3). For example, the average extrusion rate calculated for the Aucanquilcha volcanic center (0.00003 km^3/a) [*Grunder et al.*, 2006] is in fact slower than the construction rate of the Mount Givens pluton. In addition, *Grunder et al.* [2006] found that volcanism at the Aucanquilcha volcanic cluster progressed from mafic to more felsic eruptive products over time, similar to that observed in large intrusive suites and to a lesser extent, the Mount Givens Granodiorite [*Bateman and Nokleberg*, 1978].

5. Conclusions

New high-precision U-Pb zircon data indicate that the Mount Givens Granodiorite was emplaced over a period of at least 7 Ma from approximately 98 to 91 Ma. Previous growth models for the pluton [e.g., *Bateman and Nokleberg*, 1978; *McNulty et al.*, 2000] do not satisfy the range of crystallization ages in the pluton. Instead, we suggest that the pluton was constructed incrementally by small batches of magma over time, as is observed in many other plutons and intrusive suites. Using the pluton's exposed area, relief, and age range, we calculate a long-term average emplacement rate of 0.0006 km^3/a. This is similar to average rates found in other intrusive rocks but is orders of magnitude slower than magma fluxes observed in large ignimbrites. Because the Mount Givens Granodiorite is likened to monotonous intermediates, which are thought to erupt as the result of rejuvenating a slowly accumulated crystal mush, we investigated the effects of reheating events on zircon that would be present in the system. We found that even under favorable conditions, it is difficult to dissolve zircon, and thus, it is likely that ignimbrites should preserve information about long-term magma accumulation if it occurred. The presence of much older xenocrystic zircon cores, coupled with the lack of multi-Ma crystallization age ranges in zircons from monotonous intermediates, suggests that they are not efficient at dissolving zircon prior to eruption and may be the result of high flux events that preferentially end in voluminous eruptions. Conversely, low magma fluxes are conducive to accumulating and cooling small batches of magma in the crust as plutons. This activity may be reflected in the volcanic record by long-lived, small-volume volcanic fields.

Acknowledgments

Frazer was supported by grants from the UNC Department of Geological Sciences Martin Fund, Sigma Xi, and the Geological Society of America. Courtney Beck and Daniel Gurganus provided field assistance, and Jeremy Inglis and Miquela Ingalls gave useful laboratory aid. Informal reviews by Allen Glazner and Kevin Stewart on an earlier version of the manuscript helped refine the ideas presented here. We thank Bruce Watson for discussions about zircon dissolution. Editor Michael Walter, Catherine Annen, and an anonymous reviewer provided comments that led to a much stronger presentation.

References

Annen, C. (2009), From plutons to magma chambers: Thermal constraints on the accumulation of eruptible silicic magma in the upper crust, *Earth Planet. Sci. Lett.*, *284*(3–4), 409–416, doi:10.1016/j.epsl.2009.05.006.

Bachmann, O. (2010), The petrologic evolution and pre-eruptive conditions of the rhyolitic Kos Plateau Tuff (Aegean arc), *Cent. Eur. J. Geosci.*, *2*(3), 270–305, doi:10.2478/v10085-010-0009-4.

Bachmann, O., and G. W. Bergantz (2003), Rejuvenation of the Fish Canyon magma body: A window into the evolution of large-volume silicic magma systems, *Geology*, *31*(9), 789–792, doi:10.1130/G19764.1.

Bachmann, O., and G. W. Bergantz (2006), Gas percolation in upper-crustal silicic crystal mushes as a mechanism for upward heat advection and rejuvenation of near-solidus magma bodies, *J. Volcanol. Geotherm. Res.*, *149*(1–2), 85–102, doi:10.1016/j.jvolgeores.2005.06.002.

Bachmann, O., and G. W. Bergantz (2008), Rhyolites and their source mushes across tectonic settings, *J. Petrol.*, *49*(12), 2277–2285, doi:10.1093/petrology/egn068.

Bachmann, O., and M. A. Dungan (2002), Temperature-induced Al-zoning in hornblendes of the Fish Canyon magma, *Am. Mineral.*, *87*, 1062–1076.

Bachmann, O., M. A. Dungan, and P. W. Lipman (2002), The Fish Canyon magma body, San Juan volcanic field, Colorado: Rejuvenation and eruption of an upper-crustal batholith, *J. Petrol.*, *43*(8), 1469–1503, doi:10.1093/petrology/43.8.1469.

Bachmann, O., C. F. Miller, and S. L. de Silva (2007a), The volcanic-plutonic connection as a stage for understanding crustal magmatism, *J. Volcanol. Geotherm. Res.*, *167*(1–4), 1–23, doi:10.1016/j.jvolgeores.2007.08.002.

Bachmann, O., F. Oberli, M. A. Dungan, M. Meier, R. Mundil, and H. Fischer (2007b), $^{40}Ar/^{39}Ar$ and U–Pb dating of the Fish Canyon magmatic system, San Juan volcanic field, Colorado: Evidence for an extended crystallization history, *Chem. Geol.*, *236*(1–2), 134–166, doi:10.1016/j.chemgeo.2006.09.005.

Bachmann, O., B. L. A. Charlier, and J. B. Lowenstern (2007c), Zircon crystallization and recycling in the magma chamber of the rhyolitic Kos Plateau Tuff (Aegean arc), *Geology*, *35*(1), 73–76, doi:10.1130/G23151A.1.

Bateman, P. C. (1965), Geologic map of the Blackcap Mountain quadrangle, Fresno County, California, scale 1:62,500, *GQ-428*, *U.S. Geol. Surv. Rep*, Washington.

Bateman, P. C. (1992), *Plutonism in the Central Part of the Sierra Nevada Batholith, California*, *U.S. Geol. Surv. Prof. Pap.*, *1483*, 186 pp., Washington.

Bateman, P. C., and B. W. Chappell (1979), Crystallization, fractionation, and solidification of the Tuolumne Intrusive Series, Yosemite National Park, California, *Geol. Soc. Am. Bull.*, *90*(5), 465–482, doi:10.1130/0016-7606(1979)90 < 465:CFASOT > 2.0.CO;2.

Bateman, P. C., and W. J. Nokleberg (1978), Solidification of the Mount Givens Granodiorite, Sierra Nevada, California, *J. Geology*, *86*(5), 563–579.

Bateman, P. C., J. P. Lockwood, and P. A. Lydon (1971), Geologic map of the Kaiser Peak quadrangle, central Sierra Nevada, California, scale 1:62,500, *GQ-894*, *U.S. Geol. Surv. Rep.*, Washington, D. C.

Bindeman, I. N. (2003), Crystal sizes in evolving silicic magma chambers, *Geology*, *31*(4), 367–370, doi:10.1130/0091-7613(2003)031 < 0367:CSIESM > 2.0.CO;2.

Bindeman, I. N., J. W. Valley, J. L. Wooden, and H. M. Persing (2001), Post-caldera volcanism: In situ measurement of U-Pb age and oxygen isotope ratio in Pleistocene zircons from Yellowstone caldera, *Earth Planet. Sci. Lett.*, *189*(3–4), 197–206, doi:10.1016/S0012-821X(01)00358-2.

Bowring, J. F., N. M. McLean, and S. A. Bowring (2011), Engineering cyber infrastructure for U-Pb geochronology: Tripoli and U-Pb_Redux, *Geochem. Geophys. Geosyst.*, *12*, Q0AA19, doi:10.1029/2010GC003479.

Bracciali, L., S. R. Paterson, V. Memeti, and S. Rocchi (2008), Build-up of the Tuolumne batholith, California: The Johnson Granite Porphyry, in *Laccoliths, Sills, and Dykes III Conference Physical Geology of Subvolcanic Systems: Laccolith, Sills and Dykes, Elba Island, Abstracts*, edited by S. Rocchi et al., pp. 17–18, Univ. of Pisa, Pisa, Italy.

Bryan, S. E., L. Ferrari, P. W. Reiners, C. M. Allen, C. M. Petrone, A. Ramos-Rosique, and I. H. Campbell (2008), New insights into crustal contributions to large-volume rhyolite generation in the mid-Tertiary Sierra Madre Occidental Province, Mexico, revealed by U-Pb geochronology, *J. Petrol.*, *49*(1), 47–77, doi:10.1093/petrology/egm070.

Burgess, S. D., and J. S. Miller (2008), Construction, solidification and internal differentiation of a large felsic arc pluton: Cathedral Peak granodiorite, Sierra Nevada Batholith, *Geol. Soc. London. Spec. Publ.*, *304*, 203–233, doi:10.1144/SP304.11.

Burgisser, A., and G. W. Bergantz (2011), A rapid mechanism to remobilize and homogenize highly crystalline magma bodies, *Nature*, *471*, 212–215, doi:10.1038/nature09799.

Charlier, B. L. A., D. W. Peate, C. J. N. Wilson, J. B. Lowenstern, M. Storey, and S. J. A. Brown (2003), Crystallization ages in coeval silicic magma bodies: ^{238}U-^{230}Th disequililibrium evidence from the Rotoiti and Earthquake Flat eruption deposits, Taupo volcanic zone, New Zealand, *Earth Planet. Sci. Lett.*, *206*(3–4), 441–457, doi:10.1016/S0012-821X(02)01109-3.

Charlier, B. L. A., C. J. N. Wilson, J. B. Lowenstern, S. Blake, P. W. Van Calsteren, and J. P. Davidson (2005), Magma generation at a large, hyperactive silicic volcano (Taupo, New Zealand) revealed by U-Th and U-Pb systematics in zircons, *J. Petrol.*, *46*(1), 3–32, doi:10.1093/petrology/egh060.

Chesner, C. A. (1998), Petrogenesis of the Toba Tuffs, Sumatra, Indonesia, *J. Petrol.*, *39*(3), 397–438, doi:10.1093/petroj/39.3.397.

Christiansen, R. L. (2001), *The Quaternary and Pliocene Yellowstone Plateau Volcanic Field of Wyoming, Idaho, and Montana*, *U.S. Geol. Surv. Prof. Pap., 729-G*, 145 pp., Washington, D. C.

Coleman, D. S., and A. F. Glazner (1997), The Sierra crest magmatic event: Rapid formation of juvenile crust during the Late Cretaceous in California, *Int. Geol. Rev.*, *39*, 768–787, doi:10.1080/00206819709465302.

Coleman, D. S., W. Gray, and A. F. Glazner (2004), Rethinking the emplacement and evolution of zoned plutons: Geochronologic evidence for incremental assembly of the Tuolumne Intrusive Suite, California, *Geology*, *32*(5), 433–436, doi:10.1130/G20220.1.

Coleman, D. S., R. E. Frazer, R. D. Mills, A. F. Glazner, and J. M. Bartley (2013), Plutons are texturally modified primary igneous liquids, not cumulates, *Mineral. Mag.*, *77*(5), 904.

Corfu, F., J. M. Hanchar, P. W. O. Hoskin, and P. Kinny (2003), Atlas of zircon textures, in *Zircon*, *Rev. Mineral. Geochem*, vol. 53, edited by J. M. Hanchar and P. W. O. Hoskin, pp. 468–500, Mineral. Soc. Of Am., Washington, D. C., doi:10.2113/0530469.

Couch, S., R. S. J. Sparks, and M. R. Carroll (2001), Mineral disequilibrium in lavas explained by convective self-mixing in open magma chambers, *Nature*, *411*, 1037–1039, doi:10.1038/35082540.

Crisp, J. A. (1984), Rates of magma emplacement and volcanic output, *J. Volcanol. Geotherm. Res.*, *20*(3–4), 177–211, doi:10.1016/0377-0273(84)90039-8.

Cruden, A. R., and P. Launeau (1994), Structure, magnetic fabric and emplacement of the Archean Lebel Stock, SW Abitibi Greenstone Belt, *J. Struct. Geol.*, *16*(5), 677–691, doi:10.1016/0191-8141(94)90118-X.

Cruden, A. R., O. T. Tobisch, and P. Launeau (1999), Magnetic fabric evidence for conduit-fed emplacement of a tabular intrusion: Dinkey Creek Pluton, central Sierra Nevada batholith, California, *J. Geophys. Res.*, *104*(B5), 10,511–10,530, doi:10.1029/1998JB900093.

Davis, J. W. (2010), Thermochronology and cooling histories of plutons: Implications for incremental pluton assembly, PhD thesis, Univ. of North Carolina at Chapel Hill, Chapel Hill, N.C.

Davis, J. W., D. S. Coleman, J. T. Gracely, R. Gaschnig, and M. Stearns (2012), Magma accumulation rates and thermal histories of plutons of the Sierra Nevada batholith, CA, *Contrib. Mineral. Petrol.*, *163*(3), 449–465, doi:10.1007/s00410-011-0683-7.

de Saint Blanquat, M., and B. Tikoff (1997), Development of magmatic to solid-state fabrics during syntectonic emplacement of the Mono Creek granite, Sierra Nevada batholith, in *Granite: From Segregation of Melt to Emplacement Fabrics*, edited by J. L. Bouchez et al., pp. 231–252, Kluwer Academic Publishers, Amsterdam, Netherlands.

Donnelly-Nolan, J. M., B. C. Hearn, G. H. Curtis, and R. E. Drake (1981), *Geochronology and Evaluation of the Clear Lake Volcanics*, *U.S. Geol. Surv. Prof. Pap.*, *1141*, 13 pp., Washington, D. C.

Frazer, R. E., J. S. Lackey, and V. A. Valencia (2009), New U-Pb zircon ages of the granites of Dinkey Dome: Reexamining the origins of the Shaver Intrusive Suite, *Geol. Soc. Am. Abstr. Prog.*, *41*, 14.

Frey, H. M., R. A. Lange, C. M. Hall, and H. Delgado-Granados (2004), Magma eruption rates constrained by $^{40}Ar/^{39}Ar$ chronology and GIS for the Ceboruco-San Pedro volcanic field, western Mexico, *Geol. Soc. Am. Bull.*, *116*(3–4), 259–276, doi:10.1130/B25321.1.

Gelman, S. E., F. J. Gutiérrez, and O. Bachmann (2013), On the longevity of large upper crustal silicic magma reservoirs, *Geology*, *41*(7), 759–762, doi:10.1130/G34241.1.

Gilder, S., and B. A. McNulty (1999), Tectonic exhumation and tilting of the Mount Givens pluton, central Sierra Nevada, California, *Geology*, *27*(10), 919–922, doi:10.1130/0091-7613(1999)027 < 0919:TEATOT > 2.3.CO;2.

Glazner, A. F., J. M. Bartley, D. S. Coleman, W. Gray, and R. Z. Taylor (2004), Are plutons assembled over millions of years by amalgamation from small magma chambers?, *Geol. Soc. Am. Today*, *14*, 4–11.

Grunder, A. L., E. W. Klemetti, T. C. Feeley, and C. M. McKee (2006), Eleven million years of arc volcanism at the Aucanquilcha Volcanic Cluster, northern Chilean Andes: Implications for the life span and emplacement of plutons, *Trans. R. Soc. Edinb. Earth Sci.*, *97*(4), 415–436, doi:10.1017/S0263593300001541.

Guillet, P., J. L. Bouchez, and J. J. Wagner (1983), Anisotropy of magnetic susceptibility and magmatic structures in the Guérande granite massif (France), *Tectonics*, *2*(5), 419–429, doi:10.1029/TC002i005p00419.

Hamilton, W., and W. B. Myers (1967), *The Nature of Batholiths*, *U.S. Geol. Surv. Prof. Pap.*, *554-C*, 30 pp., Washington, D. C.

Henry, C. D., M. J. Kunk, and W. C. McIntosh (1994), $^{40}Ar/^{39}Ar$ chronology and volcanology of silicic volcanism in the Davis Mountains, Trans-Pecos Texas, *Geol. Soc. Am. Bull.*, *106*(11), 1359–1376, doi:10.1130/0016-7606(1994)106 < 1359:AACAVO > 2.3.CO;2.

Hildreth, W. (1979), The Bishop Tuff: Evidence for the origin of compositional zonation in silicic magma chambers, *Geol. Soc. Am. Spec. Pap.*, *180*, 45–75, doi:10.1130/SPE180-p43.

Hildreth, W. (1981), Gradients in silicic magma chambers: Implications for lithospheric magmatism, *J. Geophys. Res.*, *86*(B11), 10,153–10,192, doi:10.1029/JB086iB11p10153.

Hildreth, W. (2004), Volcanological perspectives on Long Valley, Mammoth Mountain, and Mono Craters: Several contiguous but discrete systems, *J. Volcanol. Geotherm. Res.*, *136*(3–4), 169–198, doi:10.1016/j.jvolgeores.2004.05.019.

Huang, F., C. C. Lundstrom, J. Glessner, A. Ianno, A. Boudreau, J. Li, E. C. Ferré, S. Marshak, and J. DeFrates (2009), Chemical and isotopic fractionation of wet andesite in a temperature gradient: Experiments and models suggesting a new mechanism of magma differentiation, *Geochim. Cosmochim. Acta*, *73*(3), 729–749, doi:10.1016/j.gca.2008.11.012.

Huber, C., O. Bachmann, and M. Manga (2009), Homogenization processes in silicic magma chambers by stirring and mushification (latent heat buffering), *Earth Planet. Sci. Lett.*, *283*(1–4), 38–47, doi:10.1016/j.epsl.2009.03.029.

Huber, C., O. Bachmann, and M. Manga (2010), Two competing effects of volatiles on heat transfer in crystal-rich magmas: Thermal insulation vs. defrosting, *J. Petrol.*, *51*(4), 847–867, doi:10.1093/petrology/egq003.

Huber, C., O. Bachmann, and J. Dufek (2012), Crystal-poor versus crystal-rich ignimbrites: A competition between stirring and reactivation, *Geology*, *40*(2), 115–118, doi:10.1130/G32425.1.

Jaffey, A. H., K. F. Flynn, L. E. Glendenin, W. C. Bentley, and A. M. Essling (1971), Precision measurement of half-lives and specific activities of ^{235}U and ^{238}U, *Phys. Rev. C.*, *4*(5), 1889–1906.

King, R. F. (1966), The magnetic susceptibility of some Irish granites, *Geol. J.*, *5*(1), 43–66, doi:10.1002/gj.3350050106.

Lackey, J. S., J. W. Valley, J. H. Chen, and D. F. Stockli (2008), Dynamic magma systems, crustal recycling, and alteration in the central Sierra Nevada, *J. Petrol.*, *49*(7), 1397–1426, doi:10.1093/petrology/egn030.

Lackey, J. S., M. R. Cecil, C. J. Windham, R. E. Frazer, I. N. Bindeman, and G. E. Gehrels (2012), The Fine Gold Intrusive Suite: The roles of basement terranes and magma source development in the Early Cretaceous Sierra Nevada Batholith, *Geosphere*, *8*(2), 292–313, doi:10.1130/GES00745.1.

Lanphere, M. A., and H. Baadsgaard (2001), Precise K–Ar, $^{40}Ar/^{39}Ar$, Rb–Sr and U/Pb mineral ages from the 27.5 Ma Fish Canyon Tuff reference standard, *Chem. Geol.*, *175*(3–4), 653–671, doi:10.1016/S0009-2541(00)00291-6.

Lanphere, M. A., D. E. Champion, R. L. Christiansen, G. A. Izett, and J. D. Obradovich (2002), Revised ages for tuffs of the Yellowstone Plateau volcanic field: Assignment of the Huckleberry Ridge Tuff to a new geomagnetic polarity event, *Geol. Soc. Am. Bull.*, *114*(5), 559–568, doi:10.1130/0016-7606(2002)114 < 0559:RAFTOT > 2.0.CO;2.

Leuthold, J., O. Müntener, L. P. Baumgartner, B. Putlitz, M. Ovtcharova, and U. Schaltegger (2012), Time resolved construction of a bimodal laccolith (Torres del Paine, Patagonia), *Earth Planet. Sci. Lett.*, *325–326*, 85–92, doi:10.1016/j.epsl.2012.01.032.

Lindsay, J. M., A. K. Schmitt, R. B. Trumbull, S. L. de Silva, W. Siebel, and R. Emmermann (2001), Magmatic evolution of the La Pacana Caldera system, Central Andes, Chile: Compositional variation of two Cogenetic, large-volume felsic ignimbrites, *J. Petrol.*, *42*(3), 459–486, doi:10.1093/petrology/42.3.459.

Lipman, P. W. (2000), The central San Juan caldera cluster: Regional volcanic framework, in *Ancient Lake Creede: Its Volcano-Tectonic Setting, History of Sedimentation, and Relation of Mineralization in the Creede Mining District*, Geol. Soc. Am. Spec. Pap., vol. 346, edited by P. M. Bethke and R. L. Hay, pp. 9–69, Geo. Soc. Am., Boulder, Colorado doi:10.1130/0-8137-2346-9.9.

Lipman, P. W. (2007), Incremental assembly and prolonged consolidation of Cordilleran magma chambers: Evidence from the Southern Rocky Mountain volcanic field, *Geosphere*, *3*(1), 42–70, doi:10.1130/GES00061.1.

Lundstrom, C. (2009), Hypothesis for the origin of convergent margin granitoids and Earth's continental crust by thermal migration zone refining, *Geochim. Cosmochim. Acta*, *73*(19), 5709–5729, doi:10.1016/j.gca.2009.06.020.

Lundstrom, C. C., S. Marshak, J. DeFrates, and J. Mabon (2011), Alternative processes for developing fabric and mineral compositional zoning in intrusive rocks, *Int. Geol. Rev.*, *53*(3–4), 377–405, doi:10.1080/00206814.2010.496183.

Mahood, G. A. (1990), Second reply to comment of R.S.J. Sparks, H.E. Huppert and C.J.N. Wilson on "Evidence for long residence times of rhyolitic magma in the Long Valley magmatic system: The isotopic record in the precaldera lavas of Glass Mountain, *Earth Planet. Sci. Lett.*, *99*(4), 395–399, doi:10.1016/0012-821X(90)90145-N.

Mattinson, J. M. (2005), Zircon U-Pb chemical abrasion ("CA-TIMS") method: Combined annealing and multi-step partial dissolution analysis for improved precision and accuracy of zircon ages, *Chem. Geol.*, *220*(1–2), 47–66, doi:10.1016/j.chemgeo.2005.03.011.

Matzel, J. E. P., S. A. Bowring, and R. B. Miller (2006), Time scales of pluton construction at differing crustal levels: Examples from the Mount Stuart and Tenpeak intrusions, North Cascades, Washington, *Geol. Soc. Am. Bull.*, *118*(11–12), 1412–1430, doi:10.1130/B25923.1.

Maughan, L. L., E. H. Christiansen, M. G. Best, C. S. Grommé, A. L. Deino, and D. G. Tingey (2002), The Oligocene Lund Tuff, Great Basin, USA: A very large volume monotonous intermediate, *J. Volcanol. Geotherm. Res.*, *113*(1–2), 129–157, doi:10.1016/S0377-0273(01)00256-6.

McLean, N. M., J. F. Bowring, and S. A. Bowring (2011), An algorithm for U-Pb isotope dilution data reduction and uncertainty propagation, *Geochem. Geophys. Geosyst.*, *12*, Q0AA18, doi:10.1029/2010GC003478.

McNulty, B. A., O. R. Tobisch, A. R. Cruden, and S. Gilder (2000), Multistage emplacement of the Mount Givens pluton, central Sierra Nevada batholith, California, *Geol. Soc. Am. Bull.*, *112*(1), 119–135, doi:10.1130/0016-7606(2000)112 < 119:MEOTMG > 2.0.CO;2.

Memeti, V., S. Paterson, J. Matzel, R. Mundil, and D. Okaya (2010), Magmatic lobes as "snapshots" of magma chamber growth and evolution in large, composite batholiths: An example from the Tuolumne intrusion, Sierra Nevada, California, *Geol. Soc. Am. Bull.*, *122*(11–12), 1912–1931, doi:10.1130/B30004.1.

Meyers, S. R., S. E. Siewert, B. S. Singer, B. B. Sageman, D. J. Condon, J. D. Obradovich, B. R. Jicha, and D. A. Sawyer (2012), Intercalibration of radioisotopic and astrochronologic time scales for the Cenomanian-Turonian boundary interval, Western Interior Basin, U.S.A., *Geology*, *40*(1), 7–10, doi:10.1130/G32261.1.

Miller, J. S., J. E. P. Matzel, C. F. Miller, S. D. Burgess, and R. B. Miller (2007), Zircon growth and recycling during the assembly of large, composite arc plutons, *J. Volcanol. Geotherm. Res.*, *167*(1–4), 282–299, doi:10.1016/j.jvolgeores.2007.04.019.

Mills, R. D., and D. S. Coleman (2013), Temporal and chemical connections between plutons and ignimbrites from the Mount Princeton magmatic center, *Contrib. Mineral. Petrol.*, *165*(5), 961–980, doi:10.1007/s00410-012-0843-4.

Mills, R. D., J. J. Ratner, and A. F. Glazner (2011), Experimental evidence for crystal coarsening and fabric development during temperature cycling, *Geology*, *39*(12), 1139–1142, doi:10.1130/G32394.1.

Molloy, C., P. Shane, and I. Nairn (2008), Pre-eruption thermal rejuvenation and stirring of a partly crystalline rhyolite pluton revealed by the Earthquake Flat Pyroclastics deposits, New Zealand, *J. Geol. Soc.*, *165*, 435–447, doi:10.1144/0016-76492007-071.

Mundil, R., K. R. Ludwig, I. Metcalfe, and P. R. Renne (2004), Age and timing of the Permian mass extinctions: U/Pb dating of closed-system zircons, *Science*, *305*, 1760–1763, doi:10.1126/science.1101012.

Petford, N., A. R. Cruden, K. J. W. McCaffrey, and J. L. Vigneresse (2000), Granite magma formation, transport and emplacement in the Earth's crust, *Nature*, *408*, 669–673, doi:10.1038/35047000.

Reid, M. R. (2008), How long does it take to supersize an eruption?, *Elements*, *4*, 23–28, doi:10.2113/GSELEMENTS.4.1.23.

Renne, P. R., O. T. Tobisch, and J. B. Saleeby (1993), Thermochronologic record of pluton emplacement, deformation, and exhumation at Courtright shear zone, central Sierra Nevada, California, *Geology*, *21*(4), 331–334, doi:10.1130/0091-7613(1993)021 < 0331:TROPED > 2.3.CO;2.

Rioux, M., C. J. Lissenberg, N. M. McLean, S. A. Bowring, C. J. MacLeod, E. Hellebrand, and N. Shimizu (2012), Protracted timescales of lower crustal growth at the fast-spreading East Pacific Rise, *Nat. Geosci.*, *5*, 275–278, doi:10.1038/ngeo1378.

Rose, W. I., and C. A. Chesner (1987), Dispersal of ash in the great Toba eruption, 75 ka, *Geology*, *15*(10), 913–917, doi:10.1130/0091-7613(1987)15 < 913:DOAITG > 2.0.CO;2.

Rosera, J. M., D. S. Coleman, and H. J. Stein (2013), Re-evaluating genetic models for porphyry Mo mineralization at Questa, New Mexico: Implications for ore deposition following silicic ignimbrite eruption, *Geochem. Geophys. Geosyst.*, *14*, 787–805, doi:10.1002/ggge.20048.

Schaltegger, U., P. Brack, M. Ovtcharova, I. Peytcheva, B. Schoene, A. Stracke, M. Marocchi, and G. M. Bargossi (2009), Zircon and titanite recording 1.5 million years of magma accretion, crystallization and initial cooling in a composite pluton (southern Adamello batholith, northern Italy), *Earth Planet. Sci. Lett.*, *286*(1–2), 208–218, doi:10.1016/j.epsl.2009.06.028.

Schmitt, A. K., J. M. Lindsay, S. de Silva, and R. B. Trumbull (2002), U-Pb zircon chronostratigraphy of early-Pliocene ignimbrites from La Pacana, north Chile: Implications for the formation of stratified magma chambers, *J. Volcanol. Geotherm. Res.*, *120*(1–2), 43–53, doi:10.1016/S0377-0273(02)00359-1.

Schmitz, M. D., and S. A. Bowring (2001), U-Pb zircon and titanite systematics of the Fish Canyon Tuff: An assessment of high-precision U-Pb geochronology and its application to young volcanic rocks, *Geochim. Cosmochim. Acta*, *65*(15), 2571–2587, doi:10.1016/S0016-7037(01)00616-0.

Schmitz, M. D., and B. Schoene (2007), Derivation of isotope ratios, errors, and error correlations for U-Pb geochronology using ^{205}Pb-^{235}U-(^{233}U)-spiked isotope dilution thermal ionization mass spectrometric data, *Geochem. Geophys. Geosyst.*, *8*, Q08006, doi:10.1029/2006GC001492.

Schoene, B., C. Latkoczy, U. Schaltegger, and D. Günther (2010), A new method integrating high-precision U–Pb geochronology with zircon trace element analysis (U–Pb TIMS-TEA), *Geochim. Cosmochim. Acta*, *74*(24), 7144–7159, doi:10.1016/j.gca.2010.09.016.

Schoene, B., U. Schaltegger, P. Brack, C. Latkoczy, A. Stracke, and D. Günther (2012), Rates of magma differentiation and emplacement in a ballooning pluton recorded by U-Pb TIMS-TEA, Adamello batholith, Italy, *Earth Planet. Sci. Lett.*, *355–356*, 162–173, doi:10.1016/j.epsl.2012.08.019.

Schöpa, A., and C. Annen (2013), The effects of magma flux variations on the formation and lifetime of large silicic magma chambers, *J. Geophys. Res. Solid Earth*, *118*, 926–942, doi:10.1002/jgrb.50127.

Shane, P., I. A. Nairn, V. C. Smith, M. Darragh, K. Beggs, and J. W. Cole (2008), Silicic recharge of multiple rhyolite magmas by basaltic intrusion during the 22.6 ka Okareka Eruption Episode, New Zealand, *Lithos*, *103*(3–4), 527–549, doi:10.1016/j.lithos.2007.11.002.

de Silva, S. L., and W. D. Gosnold (2007), Episodic construction of batholiths: Insights from the spatiotemporal development of an ignimbrite flare-up, *J. Volcanol. Geotherm. Res.*, *167*(1–4), 320–335, doi:10.1016/j.jvolgeores.2007.07.015.

Simon, J. I., and M. R. Reid (2005), The pace of rhyolite differentiation and storage in an 'archetypical' silicic magma system, Long Valley, California, *Earth Planet. Sci. Lett.*, *235*(1–2), 123–140, doi:10.1016/j.epsl.2005.03.013.

Stern, T. W., P. C. Bateman, B. A. Morgan, M. F. Newell, and D. L. Peck (1981), *Isotopic U-Pb ages of Zircon from the Granitoids of the Central Sierra Nevada, California*, *U.S. Geol. Surv. Prof. Pap.*, *1185*, 17 pp., Washington, D. C.

Tappa, M. J., D. S. Coleman, R. D. Mills, and K. M. Samperton (2011), The plutonic record of a silicic ignimbrite from the Latir volcanic field, New Mexico, *Geochem. Geophys. Geosyst.*, *12*, Q10011, doi: 10.1029/2011gc003700.

Tikoff, B., M. R. Davis, C. Teyssier, M. de Saint Blanquat, G. Habert, and S. Morgan (2005), Fabric studies within the Cascade Lake shear zone, Sierra Nevada, California, *Tectonophysics*, *400*(1–4), 209–226, doi:10.1016/j.tecto.2005.03.003.

Tobisch, O. T., P. R. Renne, and J. B. Saleeby (1993), Deformation resulting from regional extension during pluton ascent and emplacement, central Sierra Nevada, California, *J. Struct. Geol.*, *15*(3–5), 609–628, doi:10.1016/0191-8141(93)90151-Y.

Tobisch, O. T., J. B. Saleeby, P. R. Renne, B. McNulty, and W. Tong (1995), Variations in deformation fields during development of a large-volume magmatic arc, central Sierra Nevada, California, *Geol. Soc. Am. Bull.*, *107*(2), 148–166, doi:10.1130/0016-7606(1995)107 < 0148:VIDFDD > 2.3.CO;2.

Togashi, S., N. Miyaji, and H. Yamazaki (1991), Fractional crystallization in a large tholeiitic magma chamber during the early stage of Younger Fuji Volcano, *Bull. Volcanol. Soc. Jpn.*, *36*, 269–280.

Vazquez, J. A., and M. R. Reid (2004), Probing the accumulation history of the voluminous Toba magma, *Science*, *305*(5686), 991–994, doi:10.1126/science.1096994.

Wark, D. A., W. Hildreth, F. S. Spear, D. J. Cherniak, and E. B. Watson (2007), Pre-eruption recharge of the Bishop magma system, *Geology*, *35*(3), 235–238, doi:10.1130/G23316A.1.

Watson, E. B. (1996), Dissolution, growth and survival of zircons during crustal fusion: Kinetic principles, geological models and implications for isotopic inheritance, *Trans. R. Soc. Edinb. Earth. Sci.*, *87*(1–2), 43–56, doi:10.1017/S0263593300006465.

White, S. M., J. A. Crisp, and F. J. Spera (2006), Long-term volumetric eruption rates and magma budgets, *Geochem, Geophys. Geosyst.*, *7*, Q03010, doi:10.1029/2005GC001002.

Wilson, C. J. N. (2001), The 26.5 ka Oruanui eruption, New Zealand: An introduction and overview, *J. Volcanol. Geotherm. Res.*, *112*(1–4), 133–174, doi:10.1016/S0377-0273(01)00239-6.

Wotzlaw, J.-F., U. Schaltegger, D. A. Frick, M. A. Dungan, A. Gerdes, and D. Günther (2013), Tracking the evolution of large-volume silicic magma reservoirs from assembly to supereruption, *Geology*, *41*(8), 867–870, doi:10.1130/G34366.1.

Zimmerer, M. J., and W. C. McIntosh (2012a), An investigation of caldera-forming magma chambers using the timing of ignimbrite eruptions and pluton emplacement at the Mt. Aetna caldera complex, *J. Volcanol. Geotherm. Res.*, *245–246*, 128–148, doi:10.1016/j.jvolgeores.2012.08.007.

Zimmerer, M. J., and W. C. McIntosh (2012b), The geochronology of volcanic and plutonic rocks at the Questa caldera: Constraints on the origin of caldera-related silicic magmas, *Geol. Soc. Am. Bull.*, *124*(7–8), 1394–1408, doi:10.1130/B30544.1.

Zimmerer, M. J., and W. C. McIntosh (2013), Geochronologic evidence of upper-crustal in situ differentiation: Silicic magmatism at the Organ caldera complex, New Mexico, *Geosphere*, *9*(1), 155–169, doi:10.1130/GES00841.1.